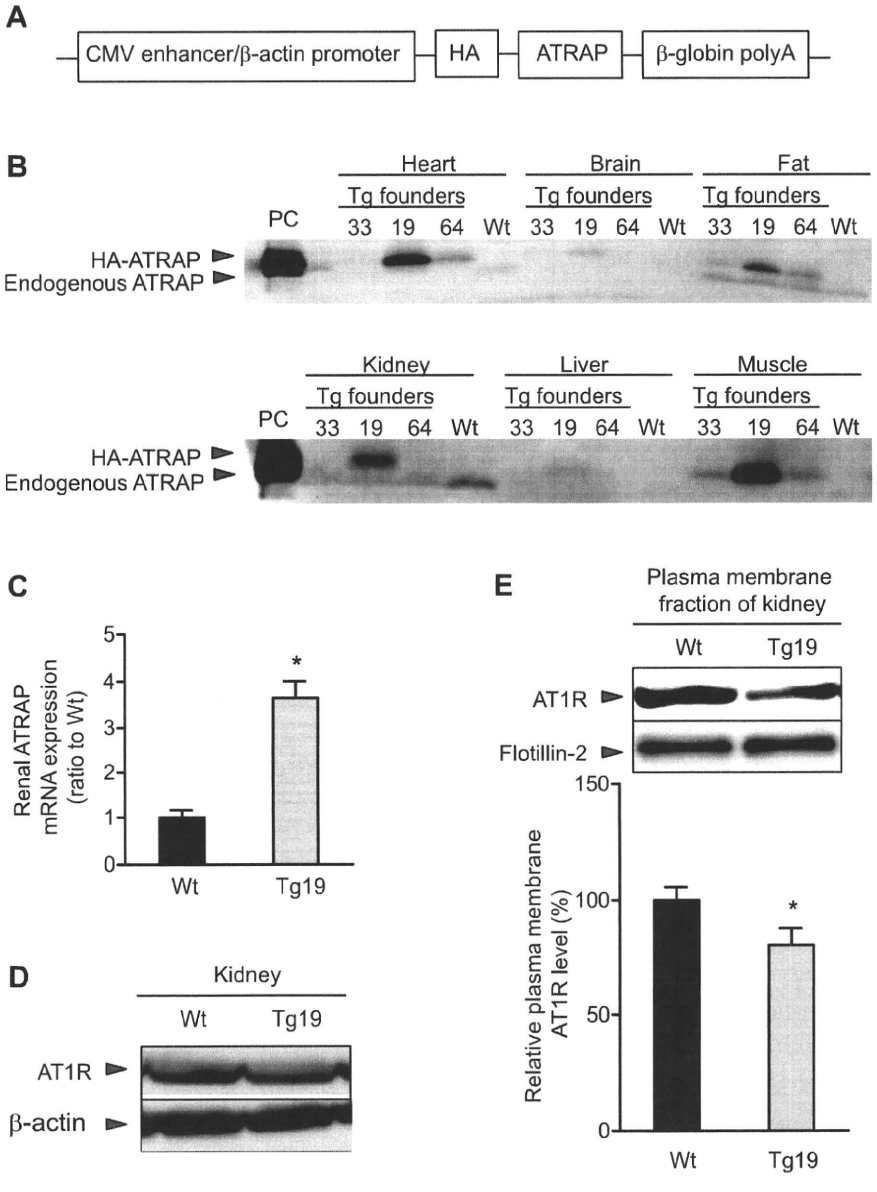

Fig. 10. Generation of ATRAP transgenic mice and decrease in the plasma membrane AT1R expression in the kidney. *A*: transgenic mice expressing ATRAP were generated on a C57BL/6J background with standard techniques. Briefly, the hemagglutinin (HA)-tagged mouse ATRAP cDNA was subcloned into the pCAGGS expression vector, which contained the cytomegalovirus (CMV) enhancer and chicken β-actin (CAG) promoter, and the resultant transgene construct was microinjected into the pronuclei of fertilized mouse embryos at the single-cell stage to generate transgenic mice (C57BL/6 strain). *B*: Western blot analysis of ATRAP expression at the protein level revealed the highest renal expression level (= 3-fold) of ATRAP (HA-ATRAP) in line 19 (Tg19), among the 3 lines of ATRAP transgene positive (+) mice obtained. Tg19 was used for further analysis in the present study. *C*: results of real-time quantitative RT-PCR analysis showed a 3.7-fold increase in the baseline renal ATRAP mRNA expression over littermate control mice (Wt) in ATRAP transgenic mice (Tg19). The values were calculated relative to those in kidneys from Wt and are expressed as means ± SE (n = 7/group). *$P < 0.05$ vs. Wt. *D*: results of Western blot analysis showed that the total kidney AT1R protein expression of Tg19 did not differ from that in Wt. *E*: results of Western blot analysis showed that the plasma membrane AT1R protein expression in the kidney of Tg19 was significantly decreased compared with Wt at baseline. The values were calculated relative to those from the plasma membrane fractions of Wt and are expressed as means ± SE (n = 9/group). *$P < 0.05$ vs. Wt.

tensinogen and α-ENaC genes in the kidney. Thus the results did not establish any causality or effect with respect to changes in renal ATRAP at this stage. Therefore, further investigation is needed to elucidate the exact molecular causal relationship between them.

The results of immunohistochemistry, including semiquantitative evaluation and Western blot analysis using the respective kidney regions, revealed a reduction of ATRAP expression in the outer medulla resulting from ANG II stimulation. Since previous studies showed that the outer medulla plays an important role in ANG II-mediated renal injury (23, 24), the suppression of renal ATRAP, particularly in the outer medullary region, may play a role in the renal pathological responses elicited by ANG II stimulation. While the intrarenal colocalization of ATRAP with AT1R suggests a functional role for ATRAP, it does not necessarily implicate ATRAP in electrolyte transport, renal injury, or hypertension, and the precise tubular function of ATRAP remains to be determined. The detailed molecular mechanism responsible for the tissue-specific AT1R-mediated suppression of ATRAP expression is still unclear. Further studies are necessary to determine the regulatory machinery of ATRAP gene transcription, including the transcription factors interacting with the promoter region of ATRAP gene and the functional effects of ATRAP on ANG II-mediated pathological responses using cultured renal tubular cells, and such studies are now underway.

Previous in vitro results suggested that ATRAP promotes AT1R internalization so as to inhibit AT1R signaling (37). In the present study, chronic ANG II infusion with either the a low or high dose caused significant suppression of endogenous ATRAP expression in the kidney, but not in the testis (Fig. 2).

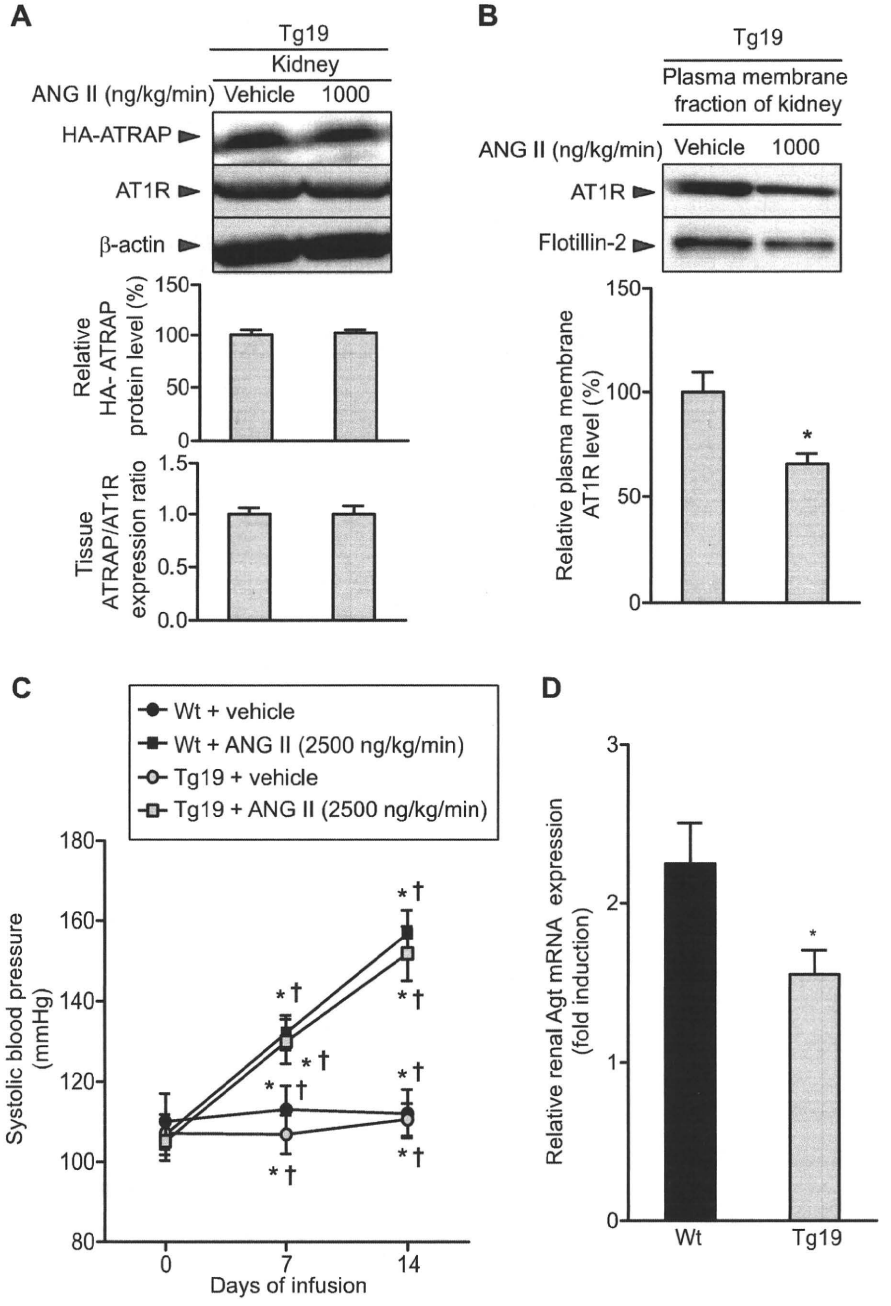

Fig. 11. Promotion of AT1R internalization and inhibition of induced expression of angiotensinogen gene in response to ANG II in the kidney of ATRAP transgenic mice. *A*: representative Western blots showing the effects of continuous ANG II infusion on the total protein expression of HA-ATRAP and AT1R in the kidney of ATRAP transgenic mice (Tg19) infused with vehicle or ANG II (1,000 $ng \cdot kg^{-1} \cdot min^{-1}$) for 14 days. Measurement of the ATRAP-to-AT1R ratio was performed as described in METHODS, and the values were calculated relative to those in extracts from Tg19 infused with vehicle and are expressed as means ± SE (n = 6/group). *B*: representative Western blots showing the effects of ANG II infusion on the plasma membrane AT1R protein level in the kidney of Tg19 infused with vehicle or ANG II (1,000 $ng \cdot kg^{-1} \cdot min^{-1}$) for 14 days. The values were calculated relative to those obtained with extracts from Tg19 infused with vehicle and are expressed as means ± SE (n = 6/group). *C*: effects of ANG II infusion on systolic blood pressure during the treatment period. Tg19 and littermate control mice (Wt) were infused with either vehicle or ANG II (2,500 $ng \cdot kg^{-1} \cdot min^{-1}$) for 14 days. The values of systolic blood pressure are expressed as means ± SE (n = 6/group). *$P < 0.05$ vs. vehicle. †$P < 0.05$ vs. *day 0*. *D*: effects of ANG II infusion on renal Agt mRNA expression in Wt and Tg19. Values are calculated as the fold-induction of those from extracts in the vehicle-infused mice and are expressed as means ± SE (n = 6/group). *$P < 0.05$ vs. Wt.

On the other hand, ANG II infusion did not alter plasma membrane AT1R expression in the kidney but significantly decreased it in the testis (Fig. 8), while total AT1R expression was not altered by ANG II in either of these tissues (Fig. 2). As a result, it is probable that testicular ATRAP promoted substantial ANG II-induced AT1R internalization, which was estimated by comparing the plasma membrane AT1R level with the total AT1R level.

In terms of AT1R internalization in the kidney, although ANG II downregulated ATRAP expression and olmesartan treatment recovered it to the baseline level (Fig. 8), the plasma membrane AT1R expression itself was not affected at all (Fig. 9), thereby still indicating the possibility that renal ATRAP exerts no effect on AT1R internalization in the kidney. We hypothesized that upregulation of renal ATRAP expression beyond baseline promotes AT1R internalization such that it is detected as a decrease in plasma membrane AT1R expression in the kidney without a change in the total AT1R protein level.

Thus, to examine the ATRAP-mediated effect on renal AT1R internalization by a different strategy in vivo, we produced ATRAP transgenic mice. The results demonstrated that enhancement of renal ATRAP expression in transgenic mice caused a decrease in the plasma membrane AT1R level, even at baseline without ANG II stimulation, irrespective of there

being no change in the total AT1R level in the kidney (Fig. 10). Furthermore, the results of ANG II infusion experiments showed that the plasma membrane AT1R level was further decreased by ANG II stimulation in the kidney of ATRAP transgenic mice (Fig. 11), which was accompanied by a decreased response of renal angiotensinogen mRNA expression to ANG II. This is in contrast to there being no change in the plasma membrane AT1R level by ANG II in the kidney of wild-type mice (Fig. 9). These results collectively suggest that enhancement of renal ATRAP expression beyond baseline promotes AT1R internalization in response to ANG II. A recent study by Oppermann et al. (29) also showed that a genetic deficiency of ATRAP in mice caused an enhanced surface expression of AT1R in the kidney, which is consistent with the results in this study.

The results of the present study show that continuous ANG II infusion decreased intrarenal ATRAP expression through ANG II-mediated AT1R signaling, particularly in the outer medulla, with the lack of any decrease in plasma membrane AT1R expression in the kidney in C57BL/6 wild-type mice. On the other hand, transgenic overexpression of ATRAP reduced the plasma membrane AT1R level in the kidney at baseline and further decreased the plasma membrane AT1R expression in response to ANG II stimulation, concomitant with the decreased ANG II-induced response of the angiotensinogen gene, despite there being no change in the total AT1R level.

Nevertheless, a limitation of the present study is that our findings strongly suggest that ATRAP at supraphysiological levels can alter the plasma membrane levels of AT1R at baseline and in response to ANG II stimulation, but with no detectable physiological effect on blood pressure. Target organ effects such as proteinuria and degree of renal damage by histological examination were not analyzed in this study. The only detectable consequence was a difference in angiotensinogen mRNA expression in response to ANG II stimulation, but it remains unclear whether this would translate to a difference in angiotensinogen protein levels.

In conclusion, these results suggest that AT1R and ATRAP modulate each other, at least in the kidney, and that activation of AT1R signaling has a dominant effect over endogenous renal ATRAP under chronic ANG II infusion, but that renal ATRAP activation by a transgenic model that increases ATRAP expression beyond baseline may cause a constitutive reduction of plasma membrane AT1R expression and a promotion of AT1R internalization in response to ANG II. Further studies to analyze downstream signaling events mediated by activation of AT1R under the condition of ATRAP overexpression are warranted to elucidate the detailed molecular mechanisms and pathophysiological significance of ATRAP-mediated inhibition of AT1R signaling in vivo.

ACKNOWLEDGMENTS

The authors thank Emi Maeda and Hiroko Morinaga for technical assistance and helpful discussion. The authors also thank Dr. Kevin Boru for English editing of this manuscript.

GRANTS

This work was supported in part by grants from the Japanese Ministry of Education, Science, Sports, and Culture, by a Health and Labor Sciences Research grant, and by grants from the Salt Science Research Foundation (1033), the Mitsubishi Pharma Research Foundation, and the Strategic Research Project of Yokohama City University.

DISCLOSURES

No conflicts of interest, financial or otherwise, are declared by the authors.

REFERENCES

1. **Azuma K, Tamura K, Shigenaga A, Wakui H, Masuda S, Tsurumi-Ikeya Y, Tanaka Y, Sakai M, Matsuda M, Hashimoto T, Ishigami T, Lopez-Ilasaca M, Umemura S.** Novel regulatory effect of angiotensin II type 1 receptor-interacting molecule on vascular smooth muscle cells. *Hypertension* 50: 926–932, 2007.
2. **Beutler KT, Masilamani S, Turban S, Nielsen J, Brooks HL, Ageloff S, Fenton RA, Packer RK, Knepper MA.** Long-term regulation of ENaC expression in kidney by angiotensin II. *Hypertension* 41: 1143–1150, 2003.
3. **Block K, Eid A, Griendling KK, Lee DY, Wittrant Y, Gorin Y.** Nox4 NAD(P)H oxidase mediates Src-dependent tyrosine phosphorylation of PDK-1 in response to angiotensin II: role in mesangial cell hypertrophy and fibronectin expression. *J Biol Chem* 283: 24061–24076, 2008.
4. **Chabrashvili T, Kitiyakara C, Blau J, Karber A, Aslam S, Welch WJ, Wilcox CS.** Effects of ANG II type 1 and 2 receptors on oxidative stress, renal NADPH oxidase, and SOD expression. *Am J Physiol Regul Integr Comp Physiol* 285: R117–R124, 2003.
5. **Coffman TM, Crowley SD.** Kidney in hypertension: guyton redux. *Hypertension* 51: 811–816, 2008.
6. **Crowley SD, Gurley SB, Herrera MJ, Ruiz P, Griffiths R, Kumar AP, Kim HS, Smithies O, Le TH, Coffman TM.** Angiotensin II causes hypertension and cardiac hypertrophy through its receptors in the kidney. *Proc Natl Acad Sci USA* 103: 17985–17990, 2006.
7. **Cui T, Nakagami H, Iwai M, Takeda Y, Shiuchi T, Tamura K, Daviet L, Horiuchi M.** ATRAP, novel AT1 receptor associated protein, enhances internalization of AT1 receptor and inhibits vascular smooth muscle cell growth. *Biochem Biophys Res Commun* 279: 938–941, 2000.
8. **Daviet L, Lehtonen JY, Tamura K, Griese DP, Horiuchi M, Dzau VJ.** Cloning and characterization of ATRAP, a novel protein that interacts with the angiotensin II type 1 receptor. *J Biol Chem* 274: 17058–17062, 1999.
9. **Gonzalez-Villalobos RA, Satou R, Seth DM, Semprun-Prieto LC, Katsurada A, Kobori H, Navar LG.** Angiotensin-converting enzyme-derived angiotensin II formation during angiotensin II-induced hypertension. *Hypertension* 53: 351–355, 2009.
10. **Gonzalez-Villalobos RA, Seth DM, Satou R, Horton H, Ohashi N, Miyata K, Katsurada A, Tran DV, Kobori H, Navar LG.** Intrarenal angiotensin II and angiotensinogen augmentation in chronic angiotensin II-infused mice. *Am J Physiol Renal Physiol* 295: F772–F779, 2008.
11. **Guo S, Lopez-Ilasaca M, Dzau VJ.** Identification of calcium-modulating cyclophilin ligand (CAML) as transducer of angiotensin II-mediated nuclear factor of activated T cells (NFAT) activation. *J Biol Chem* 280: 12536–12541, 2005.
12. **Harrison-Bernard LM, El-Dahr SS, O'Leary DF, Navar LG.** Regulation of angiotensin II type 1 receptor mRNA and protein in angiotensin II-induced hypertension. *Hypertension* 33: 340–346, 1999.
13. **Harrison-Bernard LM, Zhuo J, Kobori H, Ohishi M, Navar LG.** Intrarenal AT_1 receptor and ACE binding in ANG II-induced hypertensive rats. *Am J Physiol Renal Physiol* 282: F19–F25, 2002.
14. **Hirose T, Satoh D, Kurihara H, Kusaka C, Hirose H, Akimoto K, Matsusaka T, Ichikawa I, Noda T, Ohno S.** An essential role of the universal polarity protein, aPKClambda, on the maintenance of podocyte slit diaphragms. *PLoS One* 4: e4194, 2009.
15. **Hong SW, Isono M, Chen S, Iglesias-De La Cruz MC, Han DC, Ziyadeh FN.** Increased glomerular and tubular expression of transforming growth factor-beta1, its type II receptor, and activation of the Smad signaling pathway in the db/db mouse. *Am J Pathol* 158: 1653–1663, 2001.
16. **Hunyady L, Bor M, Balla T, Catt KJ.** Identification of a cytoplasmic Ser-Thr-Leu motif that determines agonist-induced internalization of the AT1 angiotensin receptor. *J Biol Chem* 269: 31378–31382, 1994.
17. **Iwamoto T, Kita S, Zhang J, Blaustein MP, Arai Y, Yoshida S, Wakimoto K, Komuro I, Katsuragi T.** Salt-sensitive hypertension is triggered by Ca^{2+} entry via Na^+/Ca^{2+} exchanger type-1 in vascular smooth muscle. *Nat Med* 10: 1193–1199, 2004.

18. **Kagiyama S, Matsumura K, Fukuhara M, Sakagami K, Fujii K, Iida M.** Aldosterone-and-salt-induced cardiac fibrosis is independent from angiotensin II type 1a receptor signaling in mice. *Hypertens Res* 30: 979–989, 2007.
19. **Kobori H, Nangaku M, Navar LG, Nishiyama A.** The intrarenal renin-angiotensin system: from physiology to the pathobiology of hypertension and kidney disease. *Pharmacol Rev* 59: 251–287, 2007.
20. **Kobori H, Prieto-Carrasquero MC, Ozawa Y, Navar LG.** AT1 receptor mediated augmentation of intrarenal angiotensinogen in angiotensin II-dependent hypertension. *Hypertension* 43: 1126–1132, 2004.
21. **Lopez-Ilasaca M, Liu X, Tamura K, Dzau VJ.** The angiotensin II type I receptor-associated protein, ATRAP, is a transmembrane protein and a modulator of angiotensin II signaling. *Mol Biol Cell* 14: 5038–5050, 2003.
22. **Mogi M, Iwai M, Horiuchi M.** Emerging concepts of regulation of angiotensin II receptors: new players and targets for traditional receptors. *Arterioscler Thromb Vasc Biol* 27: 2532–2539, 2007.
23. **Mori T, Cowley AW Jr.** Angiotensin II-NAD(P)H oxidase-stimulated superoxide modifies tubulovascular nitric oxide cross-talk in renal outer medulla. *Hypertension* 42: 588–593, 2003.
24. **Mori T, O'Connor PM, Abe M, Cowley AW Jr.** Enhanced superoxide production in renal outer medulla of Dahl salt-sensitive rats reduces nitric oxide tubular-vascular cross-talk. *Hypertension* 49: 1336–1341, 2007.
25. **Navar LG, Harrison-Bernard LM, Nishiyama A, Kobori H.** Regulation of intrarenal angiotensin II in hypertension. *Hypertension* 39: 316–322, 2002.
26. **Nishiyama A, Nakagawa T, Kobori H, Nagai Y, Okada N, Konishi Y, Morikawa T, Okumura M, Meda I, Kiyomoto H, Hosomi N, Mori T, Ito S, Imanishi M.** Strict angiotensin blockade prevents the augmentation of intrarenal angiotensin II and podocyte abnormalities in type 2 diabetic rats with microalbuminuria. *J Hypertens* 26: 1849–1859, 2008.
27. **Nishiyama A, Seth DM, Navar LG.** Angiotensin II type 1 receptor-mediated augmentation of renal interstitial fluid angiotensin II in angiotensin II-induced hypertension. *J Hypertens* 21: 1897–1903, 2003.
28. **Niwa H, Yamamura K, Miyazaki J.** Efficient selection for high-expression transfectants with a novel eukaryotic vector. *Gene* 108: 193–199, 1991.
29. **Oppermann M, Gess B, Schweda F, Castrop H.** Atrap deficiency increases arterial blood pressure and plasma volume. *J Am Soc Nephrol* 21: 468–477, 2010.
30. **Oshita A, Iwai M, Chen R, Ide A, Okumura M, Fukunaga S, Yoshii T, Mogi M, Higaki J, Horiuchi M.** Attenuation of inflammatory vascular remodeling by angiotensin II type 1 receptor-associated protein. *Hypertension* 48: 671–676, 2006.
31. **Prieto-Carrasquero MC, Kobori H, Ozawa Y, Gutierrez A, Seth D, Navar LG.** AT_1 receptor-mediated enhancement of collecting duct renin in angiotensin II-dependent hypertensive rats. *Am J Physiol Renal Physiol* 289: F632–F637, 2005.
32. **Reich HN, Oudit GY, Penninger JM, Scholey JW, Herzenberg AM.** Decreased glomerular and tubular expression of ACE2 in patients with type 2 diabetes and kidney disease. *Kidney Int* 74: 1610–1616, 2008.
33. **Rohrwasser A, Morgan T, Dillon HF, Zhao L, Callaway CW, Hillas E, Zhang S, Cheng T, Inagami T, Ward K, Terreros DA, Lalouel JM.** Elements of a paracrine tubular renin-angiotensin system along the entire nephron. *Hypertension* 34: 1265–1274, 1999.
34. **Sakai M, Tamura K, Tsurumi Y, Tanaka Y, Koide Y, Matsuda M, Ishigami T, Yabana M, Tokita Y, Hiroi Y, Komuro I, Umemura S.** Expression of MAK-V/Hunk in renal distal tubules and its possible involvement in proliferative suppression. *Am J Physiol Renal Physiol* 292: F1526–F1536, 2007.
35. **Shigenaga A, Tamura K, Wakui H, Masuda S, Azuma K, Tsurumi-Ikeya Y, Ozawa M, Mogi M, Matsuda M, Uchino K, Kimura K, Horiuchi M, Umemura S.** Effect of olmesartan on tissue expression balance between angiotensin II receptor and its inhibitory binding molecule. *Hypertension* 52: 672–678, 2008.
36. **Solis GP, Hoegg M, Munderloh C, Schrock Y, Malaga-Trillo E, Rivera-Milla E, Stuermer CA.** Reggie/flotillin proteins are organized into stable tetramers in membrane microdomains. *Biochem J* 403: 313–322, 2007.
37. **Tamura K, Tanaka Y, Tsurumi Y, Azuma K, Shigenaga A, Wakui H, Masuda S, Matsuda M.** The role of angiotensin AT1 receptor-associated protein in renin-angiotensin system regulation and function. *Curr Hypertens Rep* 9: 121–127, 2007.
38. **Tamura K, Umemura S, Nyui N, Yamakawa T, Yamaguchi S, Ishigami T, Tanaka S, Tanimoto K, Takagi N, Sekihara H, Murakami K, Ishii M.** Tissue-specific regulation of angiotensinogen gene expression in spontaneously hypertensive rats. *Hypertension* 27: 1216–1223, 1996.
39. **Tamura K, Umemura S, Yamakawa T, Nyui N, Hibi K, Watanabe Y, Ishigami T, Yabana M, Tanaka S, Sekihara H, Murakami K, Ishii M.** Modulation of tissue angiotensinogen gene expression in genetically obese hypertensive rats. *Am J Physiol Regul Integr Comp Physiol* 272: R1704–R1711, 1997.
40. **Tanaka Y, Tamura K, Koide Y, Sakai M, Tsurumi Y, Noda Y, Umemura M, Ishigami T, Uchino K, Kimura K, Horiuchi M, Umemura S.** The novel angiotensin II type 1 receptor (AT1R)-associated protein ATRAP downregulates AT1R and ameliorates cardiomyocyte hypertrophy. *FEBS Lett* 579: 1579–1586, 2005.
41. **Tang H, Guo DF, Porter JP, Wanaka Y, Inagami T.** Role of cytoplasmic tail of the type 1A angiotensin II receptor in agonist- and phorbol ester-induced desensitization. *Circ Res* 82: 523–531, 1998.
42. **Tsurumi Y, Tamura K, Tanaka Y, Koide Y, Sakai M, Yabana M, Noda Y, Hashimoto T, Kihara M, Hirawa N, Toya Y, Kiuchi Y, Iwai M, Horiuchi M, Umemura S.** Interacting molecule of AT1 receptor, ATRAP, is colocalized with AT1 receptor in the mouse renal tubules. *Kidney Int* 69: 488–494, 2006.
43. **Vila-Carriles WH, Kovacs GG, Jovov B, Zhou ZH, Pahwa AK, Colby G, Esimai O, Gillespie GY, Mapstone TB, Markert JM, Fuller CM, Bubien JK, Benos DJ.** Surface expression of ASIC2 inhibits the amiloride-sensitive current and migration of glioma cells. *J Biol Chem* 281: 19220–19232, 2006.
44. **Wakui H, Tamura K, Tanaka Y, Matsuda M, Bai Y, Dejima T, Masuda S, Shigenaga A, Maeda A, Mogi M, Ichihara N, Kobayashi Y, Hirawa N, Ishigami T, Toya Y, Yabana M, Horiuchi M, Minamisawa S, Umemura S.** Cardiac-specific activation of angiotensin II type 1 receptor-associated protein completely suppresses cardiac hypertrophy in chronic angiotensin II-infused mice. *Hypertension* 55: 1157–1164, 2010.
45. **Wesseling S, Ishola DA Jr, Joles JA, Bluyssen HA, Koomans HA, Braam B.** Resistance to oxidative stress by chronic infusion of angiotensin II in mouse kidney is not mediated by the AT_2 receptor. *Am J Physiol Renal Physiol* 288: F1191–F1200, 2005.
46. **Wolak T, Kim H, Ren Y, Kim J, Vaziri ND, Nicholas SB.** Osteopontin modulates angiotensin II-induced inflammation, oxidative stress, and fibrosis of the kidney. *Kidney Int* 76: 32–43, 2009.
47. **Ye M, Wysocki J, William J, Soler MJ, Cokic I, Batlle D.** Glomerular localization and expression of angiotensin-converting enzyme 2 and Angiotensin-converting enzyme: implications for albuminuria in diabetes. *J Am Soc Nephrol* 17: 3067–3075, 2006.
48. **Zhai P, Yamamoto M, Galeotti J, Liu J, Masurekar M, Thaisz J, Irie K, Holle E, Yu X, Kupershmidt S, Roden DM, Wagner T, Yatani A, Vatner DE, Vatner SF, Sadoshima J.** Cardiac-specific overexpression of AT1 receptor mutant lacking G alpha q/G alpha i coupling causes hypertrophy and bradycardia in transgenic mice. *J Clin Invest* 115: 3045–3056, 2005.
49. **Zhuo JL, Imig JD, Hammond TG, Orengo S, Benes E, Navar LG.** Ang II accumulation in rat renal endosomes during Ang II-induced hypertension: role of AT_1 receptor. *Hypertension* 39: 116–121, 2002.
50. **Zou LX, Imig JD, von Thun AM, Hymel A, Ono H, Navar LG.** Receptor-mediated intrarenal angiotensin II augmentation in angiotensin II-infused rats. *Hypertension* 28: 669–677, 1996.

Journal of Molecular and Cellular Cardiology 50 (2011) 337–345

Contents lists available at ScienceDirect

Journal of Molecular and Cellular Cardiology

journal homepage: www.elsevier.com/locate/yjmcc

Original article

Cardiac origin of smooth muscle cells in the inflow tract

Haruko Nakano [a,b,1], Estrelania Williams [a,b,2], Masahiko Hoshijima [c,3], Mika Sasaki [d,e,2], Susumu Minamisawa [f,3], Kenneth R. Chien [d,e,*,4], Atsushi Nakano [a,b,*,5]

[a] Department of Molecular Cell and Developmental Biology, University of California, Los Angeles, Los Angeles, CA 90095, USA
[b] Eli and Edythe Broad Center of Regenerative Medicine and Stem Cell Research, University of California, Los Angeles, Los Angeles, CA 90095, USA
[c] Department of Medicine, Center for Research in Biological Systems, University of California, San Diego, La Jolla, CA 92093, USA
[d] Cardiovascular Research Center, Massachusetts General Hospital, Boston, MA 02114, USA
[e] Department of Stem Cell and Regenerative Biology, Harvard University, and the Harvard Stem Cell Institute, Cambridge, MA 02114, USA
[f] Department of Science and Engineering, Waseda University, Tokyo 169-8555, Japan

ARTICLE INFO

Article history:
Received 12 August 2010
Received in revised form 14 September 2010
Accepted 12 October 2010
Available online 23 October 2010

Keywords:
Cardiogenesis
Myogenic progenitor
Smooth muscle
Great vessel
Plasticity

ABSTRACT

Multipotent Isl1$^+$ heart progenitors give rise to three major cardiovascular cell types: cardiac, smooth muscle, and endothelial cells, and play a pivotal role in lineage diversification during cardiogenesis. A critical question is pinpointing when this cardiac–vascular lineage decision is made, and how this plasticity serves to coordinate cardiac chamber and vessel growth. The posterior domain of the Isl1-positive second heart field contributes to the SLN-positive atrial myocardium and myocardial sleeves in the cardiac inflow tract, where myocardial and vascular smooth muscle layers form anatomical and functional continuity. Herein, using a new atrial specific SLN-Cre knockin mouse line, we report that bipotent Isl1$^+$/SLN$^+$ transient cell population contributes to cardiac as well as smooth muscle cells at the heart-vessel junction in cardiac inflow tract. The Isl1$^+$/SLN$^+$ cells are capable of giving rise to cardiac and smooth muscle cells until late gestational stages. These data suggest that the cardiac and smooth muscle cells in the cardiac inflow tract share a common developmental origin. This article is part of a special issue entitled, "Cardiovascular Stem Cells Revisited".

1. Introduction

The cardiac, smooth muscle and endothelial cells arise from single, common multipotent precursor cells during embryogenesis [1–3]. Whereas three major cardiovascular lineages can arise from Flk1$^+$/Bry$^+$ mesodermal progenitors [1,4] and Flk1$^+$/Isl1$^+$/Nkx2.5$^+$ cardiogenic colonies derived from mouse embryos around E8.0–8.5 [2], smooth muscle cell lineages can also arise from c-kit$^+$/Nkx2.5$^+$ cardiac progenitor cells isolated from a later stage [3]. These progenitor populations may represent discrete lineages that constitute the heart [5]. Alternatively, they may represent cells in the same lineage at different developmental stages. The comparison of these analyses suggests that the endothelial lineage separates from the myogenic lineage at an early stage, whereas cardiac and smooth muscle lineages are closely related until later stages of cardiogenesis [6,7]. Given that the plasticity of progenitors becomes progressively restricted as embryogenesis proceeds, intriguing questions are which population displays cardiac-smooth muscle bipotency, how long the progenitors maintain their plasticity during cardiogenesis and what is the biological implication of smooth muscle differentiation capability of the cardiac progenitors.

The second heart field (SHF) is delineated by the expression of Isl1, a member of the LIM-homeodomain transcription factor family. This extra-crescent cardiac population is specified in the anterior lateral plate mesoderm adjacent to the first heart field (FHF) in the cardiac crescent [7–9]. After the FHF forms a single straight primitive heart tube, the SHF progenitors migrate from the splanchnic mesoderm towards the primitive heart tube and trigger its right-ward looping. These SHF progenitors continue to migrate and add additional myocardium to the primitive heart tube until midgestational stages. The SHF progenitors downregulate Isl1 expression immediately after completing their migration, which makes Isl1 a suitable marker of an immature state for cardiac progenitors. During this step, the Isl1$^+$ cardiac progenitors in the anterior region of the SHF (aSHF, also known as anterior heart field; AHF) migrate to the arterial pole of the heart tube and form the outflow tract and right ventricle [10–12]. This anterior subpopulation is distinguishable from other subpopulations of Isl1-positive SHF progenitors by several molecular markers

* Corresponding authors. K.R. Chien is to be contacted at Cardiovascular Research Center, Massachusetts General Hospital, Boston, MA 02114, USA. A. Nakano, Department of Molecular Cell and Developmental Biology, University of California, Los Angeles, Los Angeles, CA 90095, USA. Tel.: +1 310 267 1897.
E-mail addresses: kchien@partners.org (K.R. Chien), anakano@ucla.edu (A. Nakano)

[1] Conception and design, collection and/or assembly of data, data analysis and interpretation, manuscript writing.
[2] Collection and/or assembly of data.
[3] Conception and design, data analysis and interpretation.
[4] Conception and design, data analysis and interpretation, manuscript writing.
[5] Conception and design, collection and/or assembly of data, data analysis and interpretation, manuscript writing.

0022-2828/$ – see front matter © 2010 Elsevier Ltd. All rights reserved.
doi:10.1016/j.yjmcc.2010.10.009

including specific enhancers of Mef2c [13] and FGF10 [10], suggesting that Isl1-positive cells are already heterogeneous at this stage. The $Isl1^+$ progenitors in the aSHF eventually acquire a ventricular phenotype and contribute to the myocardium of the outflow tract and the right ventricle. Interestingly, this population also developmentally gives rise to smooth muscle cells in the root of the aorta [14]. On the other hand, Isl1-positive progenitors in posterior part of the SHF (pSHF) populate the venous pole of the primary heart tube slightly later, maintain high proliferative and migratory activity, and express Isl1 until midgestational stages [15,16]. This posterior subpopulation of late Isl1-positive progenitors eventually acquires an atrial phenotype and contributes to the myocardium in atrial chambers and myocardial sleeves in the inflow tract. Thus, at the linear heart tube stage, the $Isl1^+$ cardiac progenitor population seems to be a pool of several different subsets of cardiac progenitors including aSHF and pSHF populations. Whereas Isl1-positive progenitors in the outflow tract/arterial pole/aSHF are known to give rise to both cardiac and smooth muscle cells, it is not clear if myocardium and smooth muscle in the inflow tract share a common cellular origin in the venous pole/pSHF. This is in part because of the lack of a specific lineage marker and in part because of the lack of single cell analysis.

Sarcolipin (SLN) is an inhibitor of sarco(endo)plasmic reticulum Ca^{2+}-ATPase (SERCA) that is specifically expressed in atrial myocardium and skeletal muscle, and implicated in atrial specific contractile function [17–19]. SLN expression is gradually upregulated as the atrial myocytes maturate, and is a useful marker for the atrial muscle lineage.

Here, we report the generation of atrial specific SLN-Cre knockin mouse line, and the identification of $Isl1^+/SLN^+$ cells in the atrial lineage which contribute to atrial cardiomyocytes and smooth muscle cells in the cardiac inflow tract. To investigate the differentiation capability of $Isl1^+/SLN^+$ cells, we generated an atrial specific deleter mouse line by introducing Cre recombinase into the SLN locus. SLN-labeled atrial cells distribute in working and SA nodal atrial myocytes, as well as the smooth muscle cells in the cardiac inflow tract. *In vitro* assays indicate that $Isl1^+/SLN^+$ cells are capable of clonally differentiating into cardiomyocytes and smooth muscle cells from single progenitors. Interestingly, $Isl1^+/SLN^+$ cells retain smooth muscle competency until late gestational stages. These observations provide an insight into the origin of cardiac and smooth muscle cells at the boundary of the atrial chamber and inflow tract, and the mechanism underlying the formation of heart-vessel junctions.

2. Materials and methods

2.1. Generation of SLN-Cre mice

Exon 2 of the *SLN* locus including the 1st ATG was replaced with Cre cDNA. A correctly targeted R1 ES clone was screened by Southern blotting and genomic PCR. The recombination efficiency was 1/300 clones.

2.2. Preparation of cardiac mesenchymal feeder layer

Neonatal hearts were predigested with 0.5 mg/ml trypsin in HBSS at 4 °C overnight followed by strong digestion with collagenase at 37 °C for 1 h (0.5 mg/ml in HBSS). Cardiac mesenchymal fibroblasts were separated from myocytes by differential plating for 1 h twice. Fibroblasts from the first and the second differential plating were combined, grown until confluent and treated with 10 μg/ml mitomycin C for 2 h on the day before progenitors were seeded. The contamination of myocytes in the fibroblast fraction was less than 0.07% by cTnT staining.

2.3. Histology and immunostaining

Whole mount and section Xgal stainings were performed according to standard protocols. Double staining for Xgal and specific antibodies were performed as follows: 8 μm frozen sections or cells were stained with Xgal followed by postfixation for 5 min, 0.3% hydrogen peroxide treatment for 15 min, blocking with 10% normal goat serum for 1 h and antibody reaction in 3% normal goat serum at 4 °C overnight. Secondary antibody reaction was performed with Vectastain ABC kit (Vector lab) according to the manufacturer's protocol. Section Xgal/Isl1 staining was performed as previously described [20]. The concentrations of the primary antibodies are as follows: cTnT (1:200, Lab Vision Corp., Fremont, CA), smMHC (1:500, Biomedical Technologies Inc., Stoughton, MA), Isl1 (1:200, DSHB, Iowa City, IA), and DsRed (1:500, Clontech, Mountain View, CA).

2.4. RT-PCR and qPCR

RNA was extracted with Trizol (Invitrogen, Carlsbad, CA) or Absolute nanoprep kit (Stratagene, Ceder Creek, TX) according to the manufacturer's protocol, and cDNAs were synthesized with iScript kit (BioRad, Hercules, CA). Colony PCR was run for 35 cycles. Quantitative PCR was performed with the SYBR Green system and i-Cycler (BioRad, Hercules, CA).

2.5. Electron microscopic analysis

The $SLN^{cre/+}$; *R26R* hearts were dissected and fixed in 1% PFA and 2.5% glutaraldehyde in PBS for 3 h, and stained for 4 h in Bluo-gal staining solution; 1 mg/ml Bluo-gal (Sigma), 10 mM ferro/ferri cyanide, 2 mM MgCl2, 0.02% NP40 and 0.01% NaDOC. Stained tissues were post-fixed for 30 min in a mixture of 1% osmium tetroxide and 2% glutaraldehyde in 0.15 M cacodylate buffer (on ice), washed several times in PBS, and dehydrated in graded ethanol and acetone (all steps on ice). Preparations were left overnight in a 1:1 mixture of Epon and acetone and then for 5–10 h in unpolymerized Epon. They were transferred to molds, oriented and placed at 60 °C for 24 h to permit polymerization of the Epon. Sections were mounted on net grids (Ted Pella) and treated with uranyl acetate and lead citrate.

3. Results

3.1. SLN-Cre knockin strain is a sensitive and specific deleter line for the atrial lineage

To generate an atrial specific Cre line driven by an internal promoter, we introduced Cre recombinase by homologous recombination into exon 2 of the *SLN* locus (Figs. 1A, B, C). $SLN^{cre/+}$ heterozygotes displayed no morphological or fertility defects. While SLN mRNA is expressed at E10.0 (Fig. 2A), the βgal activity in $SLN^{cre/+}$; *R26R* embryos was first detected in the atria at around E10.5, when Isl1 is still positive in the atrial lineage (Fig. 2B). After E12.5, the atrial myocardium was broadly and strongly labeled by R26R and CAG-DsRed reporter lines [21,22] (Figs. 2C–H″, and S1A, B). Section Xgal staining of the neonatal hearts revealed that the vast majority of the atrial myocytes were labeled (Figs. 2E, F), whereas none of the endocardial or epicardial cells were stained (Fig. 2F, arrowheads; Supplemental Table 1). Interestingly, HCN4-positive SA nodal cells were also labeled by SLN-Cre (Fig. S2). These data suggest that the SLN-Cre line is a sensitive and specific deleter line for the atrial lineage. To our knowledge, this mouse is the first deleter line in which Cre recombinase is driven by an internal atrial specific promoter.

Xgal staining in the inflow region visualized the anatomical distribution of the myocardial sleeves of the venae cavae and pulmonary veins. The Xgal staining extended up to bifurcation of the internal jugular and subclavian veins in the cranial region, and

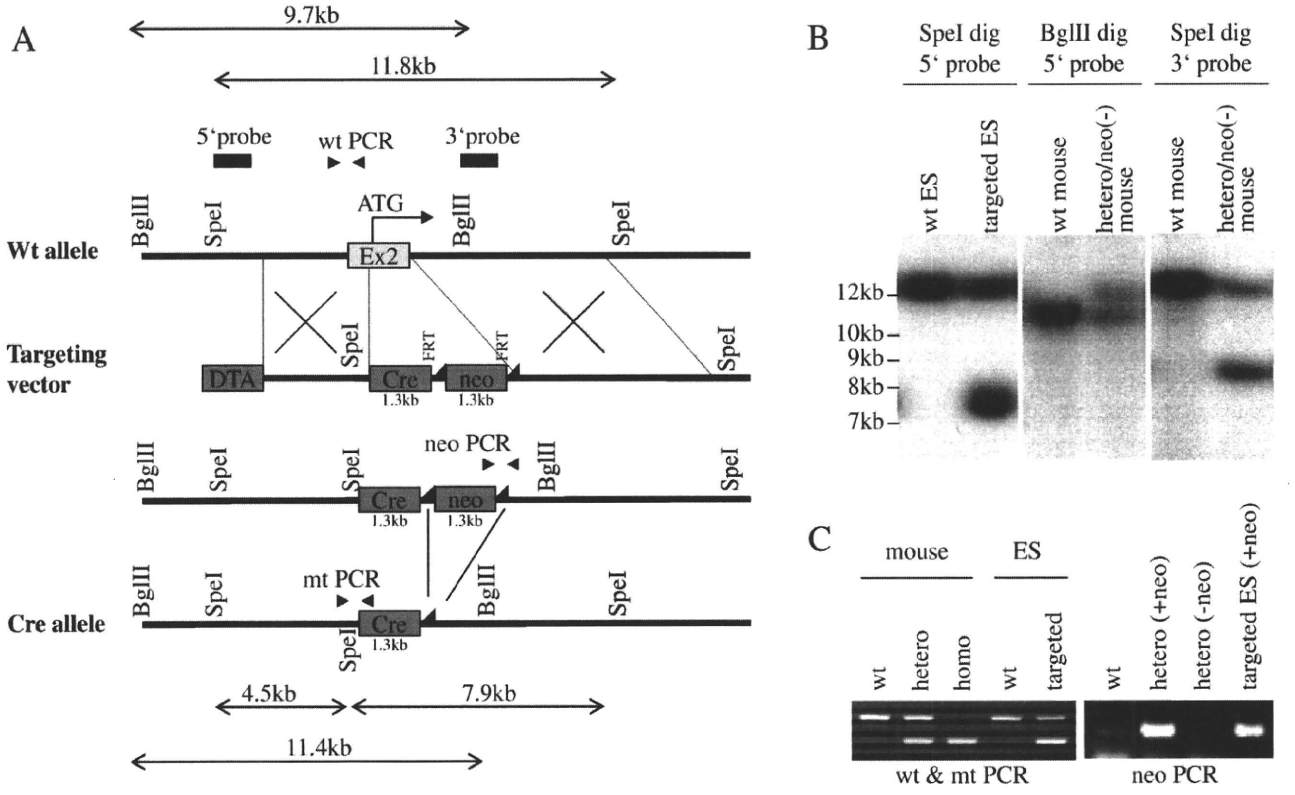

Fig. 1. Generation of SLN-Cre knockin mouse line. (A) Schematic of *SLN* genomic locus, targeting vector design and recombinant alleles. Exon 2 which includes the start codon was replaced by Cre recombinase and neomycin resistant cassette by homologous recombination. FRT sites are indicated by filled triangles. DTA, diphtheria toxin A cassette. (B) Genomic Southern blot analysis of targeted ES cells and heterozygous mouse after removal of neo cassette using 5′ and 3′ probes shown in A. (C) Genomic PCR for mouse genotyping. Primer designs are shown in A.

down to the diaphragm in the thoracic cavity (Figs. 2I–K and S1C). The boundary of the right atrium and the venae cavae is demarcated by venous valves that also are derived from *SLN*-expressing cells (Fig. 3A, arrowhead). Whereas the muscular layer of the atrial chamber consists only of myocardial cells, the muscular wall of the venae cavae distal to the venous valves consist of two muscular layers—the outer myocardial layer derived from SLN-expressing cells and inner smooth muscle layer positive for smMHC, a definitive marker for vascular smooth muscle cells (Fig. 3A). The myocardial layer tapers off towards the periphery and generates myocardial sleeves in the great veins. Similar to the vena cavae, the proximal region of the pulmonary veins also showed a two-layer structure with outer myocardial sleeve and inner smooth muscle layer (Fig. S3).

3.2. SLN-positive cells give rise to smooth muscle cells in cardiac inflow tract

Further analysis of this two-layer structure revealed the close relationship between cardiac and smooth muscle lineages during cardiovascular development. Double staining of serial sections showed that about 5–10% of smMHC-positive cells in the inflow region are co-stained with Xgal (Figs. 3C, D, black arrows; Supplemental Table 1). To confirm this, the inflow region of the atrium from $SLN^{cre/+}$; *R26R* adult mice was enzymatically dissociated and cultured on a fibronectin-coated dish. Consistent with section stainings, a fraction of βgal-labeled cells were co-stained for smMHC (Fig. 3B). Furthermore, electron microscopic analysis of Bluo-gal-stained $SLN^{cre/+}$; *R26R* hearts revealed that the smooth muscle cells with non-striated myofilaments are labeled with Bluo-gal deposits on their membranes (Figs. 3E, E′, arrowheads). βGal-labeled smooth muscle cells were also found in myocardial sleeves in the pulmonary veins (Fig. S3). These data suggest the developmental contribution of SLN-positive cells to the smooth muscle cells in the cardiac inflow tract. It has been reported that *SLN* mRNA is expressed strongly in atria and esophageal muscle and least abundantly in skeletal muscle and bladder, but no expression has been detected in vascular smooth muscle [18]. Consistently, our SLN-Cre lineage tracing experiments fail to detect any Xgal-positive smooth muscle cells in aortic or other major vasculature. Therefore, our findings raise the possibility that these two different cell types in the cardiac inflow region share a common cellular origin during cardiogenesis.

3.3. $Isl1^{+}/SLN^{+}$ cells represent a transient cell population in the venous pole

To examine the cellular origin of cardiac and smooth muscle cells in the inflow tract, we searched for Isl1-positive cells in the atrial lineage. As *in situ* hybridization and lineage tracing experiments indicated that SLN is expressed from E10.0 and on in the atria (Fig. 2A), and Isl1 expression continues until midgestation [15], we speculated that there is a spatial and temporal overlap of these two markers in the forming atria. Double staining for Xgal and Isl1 on $SLN^{cre/+} \times R26R$ embryos revealed Isl1/SLN double positive cells in forming atria (Fig. 4). At E10.5, immature cardiac progenitors with strong Isl1 expression were found in the splanchnic mesoderm (Fig. 4A, arrowheads). Cells in the primary atrial septum are also positive for Isl1 (Fig. 4A, white arrow). A subset of

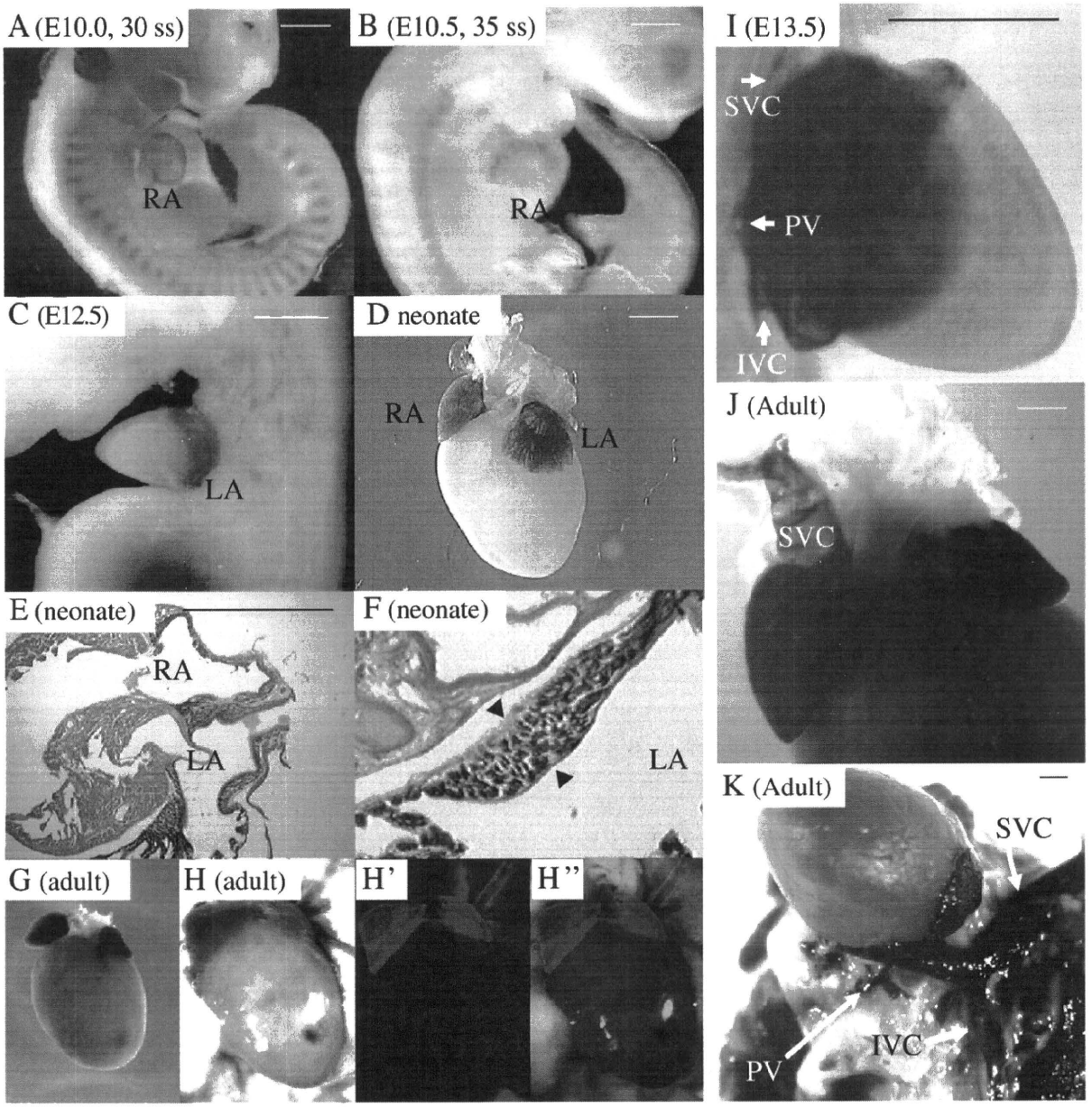

Fig. 2. *In vivo* atrial lineage tracing. (A) *In situ* hybridization for *SLN* at the 30 somite stage. *SLN* is expressed in atria and myotomes. (B–H″) Contribution of SLN^+ cells to atrial myocardium. Atrial specific labeling is shown by whole mount Xgal staining at E10.5 (B), E12.5 (C), neonatal (D) and adult (G) stages, and section Xgal staining of neonatal hearts (E, F) of *SLN-cre; R26R* mice. Note that the vast majority of the atrial myocytes are labeled. As indicated by black arrowheads, there were no Xgal-positive cells in endocardium or epicardium. H, H′ and H″ show the hearts from adult *SLN-cre; CAG-DsRed reporter* mice. The expression of βgal and DsRed reporters is restricted to atrial myocytes throughout cardiogenesis and in the adult heart. Scale bar = 1 mm. (I–K) Contribution of SLN^+ cells to the cardiac inflow tract. Whole mount Xgal staining of the inflow tract of $SLN^{cre/+}$; *R26R* embryo at E13.5 (I) and adult heart (J, K) shows that the proximal part of the SVC, IVC and PV are derived from SLN-positive cells (white arrows in I and K). Scale bar = 1 mm. IVC, inferior vena cava; LA, left atrium; PV, pulmonary vein; RA, right atrium; SVC, superior vena cava.

cardiac cells in the atrial chamber and sinus venosus have already started to express SLN, and some are positive for both Isl1 and SLN (Fig. 4A, black arrows). At E13.5, $Isl1^+$ cells in the splanchnic mesoderm are still negative for SLN (Fig. 4B, black arrowheads), although most of the atrial myocytes were already positive for βgal activity. $Isl1^+/SLN^+$ cells were still found in dorsal mesenchymal protrusion (Fig. 4B, black arrows) [15,23–28]. These cells gradually lose Isl1 expression and progressively acquire SLN as they migrate towards the cushion (Fig. 4B, black arrows). These data suggest that a subset of $Isl1^+$ cells give rise to SLN^+ atrial myocytes, and that $Isl1^+/SLN^+$ cells represent a transient cell population that are committed to the mature atrial myocyte fate.

3.4. Single $Isl1^+/SLN^+$ cells give rise to both cardiac and smooth muscle cells

To examine whether cardiac and smooth muscle lineages can originate from a single common $Isl1^+/SLN^+$ cell, we dissected forming atrial tissue from E9.5 $SLN^{cre/+}$; *R26R* embryos, dissociated them into single cells and cultured them at clonal density on cardiac mesenchymal feeder layers as previously described (Fig. 5A) [2,29,30]. βGal-labeled atrial cells grew to form colonies, and more than 90% of them were positive for Isl1 (Figs. 5B, D and Supplementary Table 2). Using a *CAG-DsRed reporter* line [22], the atrial progenitor colonies were

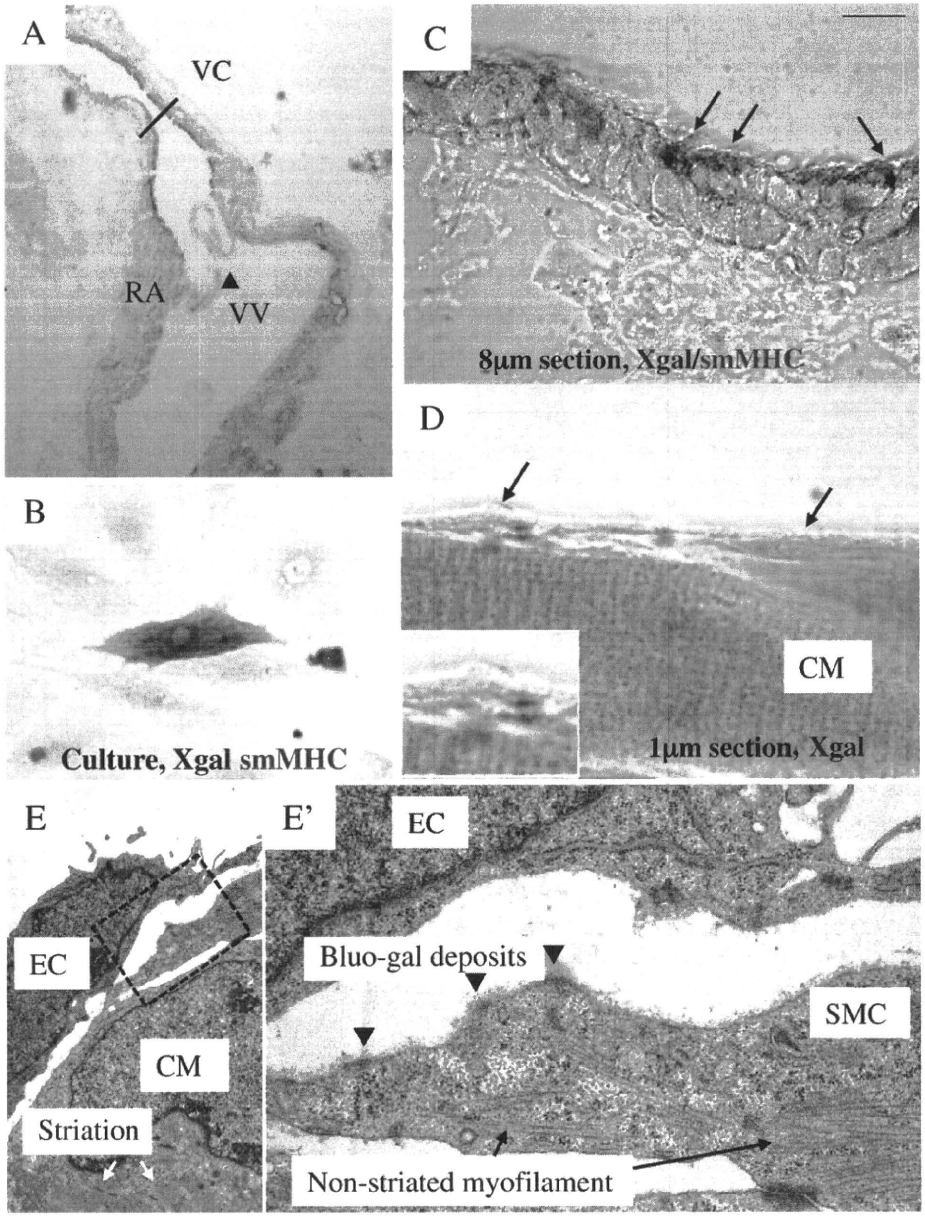

Fig. 3. SLN-positive cells give rise to smooth muscle cells in the cardiac inflow tract. (A) Low magnification view of the junction between right atrium and vena cava of adult *SLN*$^{cre/+}$; *R26R* mouse co-stained with Xgal and smMHC. The proximal region of the vena cava (VC) consists of two muscular layers; Xgal-positive outer myocardial layer (blue) and smMHC-positive inner smooth muscle layer (brown), and demarcated from the right atrium (RA) by venous valves (VV, arrowhead) which are also derived from SLN-positive cells. (B) Expression of a smooth muscle marker in βgal-labeled cells isolated from the cardiac inflow region of adult *SLN*$^{cre/+}$; *R26R* mice. Tissues from the vena cava of adult *SLN*$^{cre/+}$; *R26R* mouse were dissociated and plated onto a culture dish. Some cells express both βgal (blue) and smMHC (brown), suggesting that a fraction of SLN-positive cells gave rise to smooth muscle cells in the inflow tract. (C) Smooth muscle cells derived from SLN-expressing cells. Light microscopic analysis of 8 μm sections shows the smMHC-positive cells in the inner layer co-stained with Xgal (scale bar = 50 μm). Sections were cut along the line indicated in A. (D) 1 μm sections show clear Xgal staining on smooth muscle cells (arrows) between a thin endothelial layer and a thick myocardial layer (CM) (scale bar = 20 μm). Sections were cut along the line indicated in A. (E, E′) Electron microscopic analysis (×49,500) of the vena cava of adult *SLN*$^{cre/+}$; *R26R* mouse stained with Bluo-gal. Bluo-gal deposits (arrowheads) are found in smooth muscle cells (SMC) with non-striated myofilaments (black arrows). Note that the cardiomyocytes have striated myofilaments (white arrow). CM, cardiomyocyte; col, collagen fiber; EC, endothelial cell; SMC, smooth muscle cell; MF, myofilament; RA, right atrium; VC, vena cava; VV, venous valve.

visualized alive (Fig. 5C), picked up under the fluorescent microscope, and examined for their mRNA expression signature. After 3–4 days on feeders, the majority of the clones (early-stage colonies) were positive for early cardiac markers (Isl1, Nkx2.5, and GATA4) and atrial markers (SLN and MLC2a) (Fig. 5D). However, the expression of ANF and smMHC were only occasionally found at this stage. Therefore, the feeder system is useful for propagating immature atrial cells *in vitro*.

After differentiation for 7–12 days in culture, most of the βgal-labeled cells express cTnT. However, cTnT-negative cells were also found in the periphery of the βgal-labeled colonies (Fig. 5E, black arrow). These peripheral cells were co-stained with Xgal/smMHC (Fig. 5E, white arrows). RT-PCR revealed that no colony was positive for Isl1 at this stage (Fig. 5G). Whereas all the clones examined gave rise to cTnT-positive cardiomyocytes, 51.3% of them were capable of

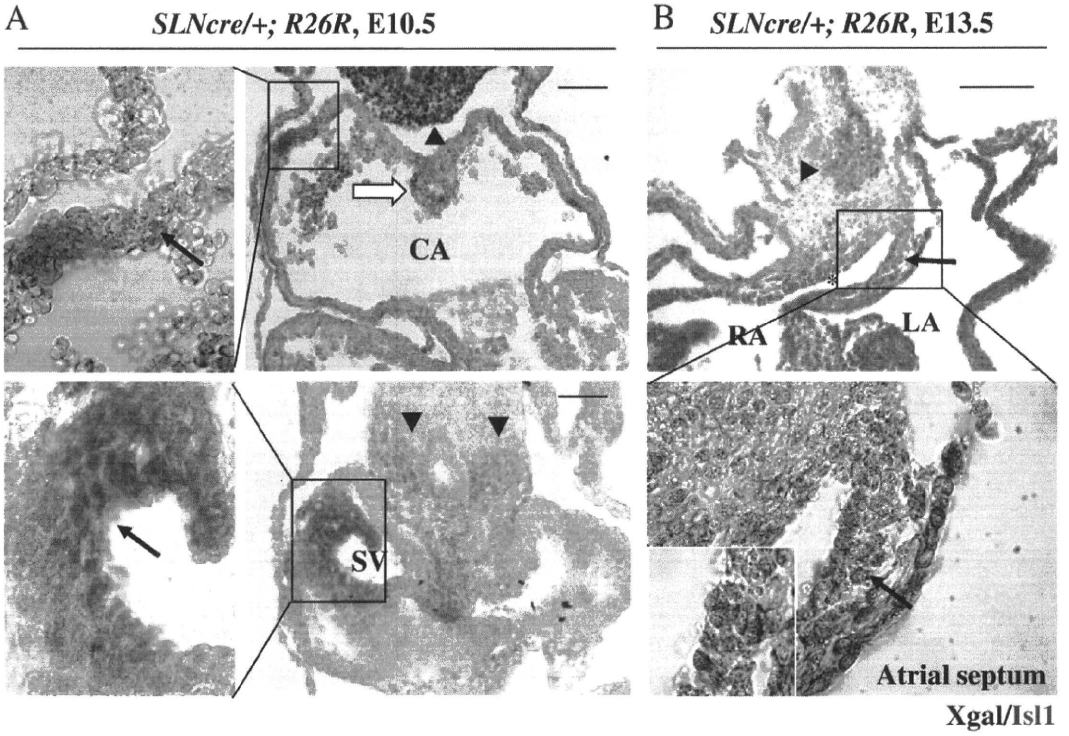

Fig. 4. Identification of Isl1$^+$/SLN$^+$ cells during cardiogenesis. Heart sections from *SLN$^{cre/+}$; R26R* embryo at E10.5 (A) and E13.5 (B) were double-stained for Xgal and Isl1. Scale bar = 100 μm. (A) At E10.5, most of the Isl1-positive cells in forming atria are negative for Xgal. Whereas cells in the splanchnic mesoderm (black arrowheads) and primary atrial septum (white arrow) strongly express Isl1, Xgal-positive cells with a weaker level of Isl1 are also seen in atrial free wall and sinus venosus (arrows). (B) At E13.5, most of the atrial myocytes have already started to express SLN. Isl1-positive immature cardiac progenitors in the splanchnic mesoderm (arrowhead) migrate into the septum and start to express SLN while maintaining Isl1 expression (black arrow). During the migration, atrial cells gradually lose Isl1 expression and gradually express SLN. CA, common atrium; LA, left atrium; RA, right atrium; SV, sinus venosus.

giving rise to smMHC-positive cells (Fig. 5G and Supplementary Table 2). Given that 90.3% of the colonies express both Isl1 and SLN, these data suggest that more than half of the Isl1$^+$/SLN$^+$ cells at E9.5 are capable of giving rise to both cardiac and smooth muscle cells. To examine the destination of Isl1$^+$/SLN$^+$ cells, DsRed-labeled cells were propagated for 7–12 days on feeders, and FACS-sorted onto glass slides by cytospin for smooth muscle staining. As shown in Fig. 5H, 3.1% of the progeny of atrial cells gave rise to smMHC-positive smooth muscle cells *ex vivo* consistent with *in vivo* lineage tracing data (Supplemental Table 1). These data suggest that while more than half of Isl1$^+$/SLN$^+$ cells are smooth muscle competent, not all of them actually give rise to smooth muscle cells.

Interestingly, atrial colonies derived from a later stage (E12.5 and 15.5) showed a decrease in smooth muscle differentiation capability (Supplementary Table 2), suggesting that smooth muscle competency is gradually restricted as the atrial myocytes mature.

Taken together, these data suggest that Isl1-positive cells in the atrial lineage contribute to cardiac as well as smooth muscle cells in the cardiac inflow tract during migration from splanchnic mesoderm.

In conclusion, we reported (1) a novel Cre mouse line which specifically and sensitively labels the atrial cardiac lineage, (2) the developmental contribution of the atrial cells into the smooth muscle cells in cardiac inflow tract, (3) the smooth muscle competency of immature atrial cells, and (4) the gradual loss of smooth muscle competency during cardiogenesis. Together, these findings provide an insight into the mechanism underlying the formation of the boundary between atrial myocardium and vascular smooth muscle layer. The myocardial–smooth muscle junction in the vena cava is often affected in some types of congenital heart disease. Moreover, the myocardial sleeve in pulmonary vein is highly arrhythmogenic in diseased and/or aged hearts. Elucidating how the plasticity of heart progenitors serves the cardiovascular morphogenesis will provide a better understanding of the pathogenesis of these diseases.

4. Discussion

The heart is the first functional organ that develops during embryogenesis, and it is unique in that it has to be operational while it is still forming. Therefore, the embryonic heart needs to strike a delicate balance between its formation and its functionality, which accounts for the fact that 1% of human live births are complicated by congenital heart diseases. A major question in cardiogenesis research is how this balance is regulated at the cellular level.

Using a newly generated atrial specific SLN-Cre knockin mouse line, we have demonstrated that the atrial subset of Isl1-positive SHF progenitors are capable of giving rise to both cardiac and smooth muscle cells until unexpectedly later stages. During the migration from splanchnic mesoderm, a majority of Isl1$^+$/SLN$^+$ cells contribute to the atrial myocardium, while a subset of them are incorporated into the inner layer of the inflow tract and give rise to smooth muscle cells (Fig. 6). Instead of making binary cell fate decision at certain developmental stages, our data suggest that the atrial cells gradually lose their plasticity during cardiogenesis.

4.1. Diversification of atrial cell populations

The SHF has been characterized by several different techniques; dye injection, detection of specific markers and retrospective single cell fate tracing experiments. Different methods and different markers have determined slightly different populations of the cardiac lineages [8,10–12,31]. Atrial cells arise from the posterior part of Isl1-positive heart field [16,27,28]. The Isl1$^+$/SLN$^+$ progenitors represent

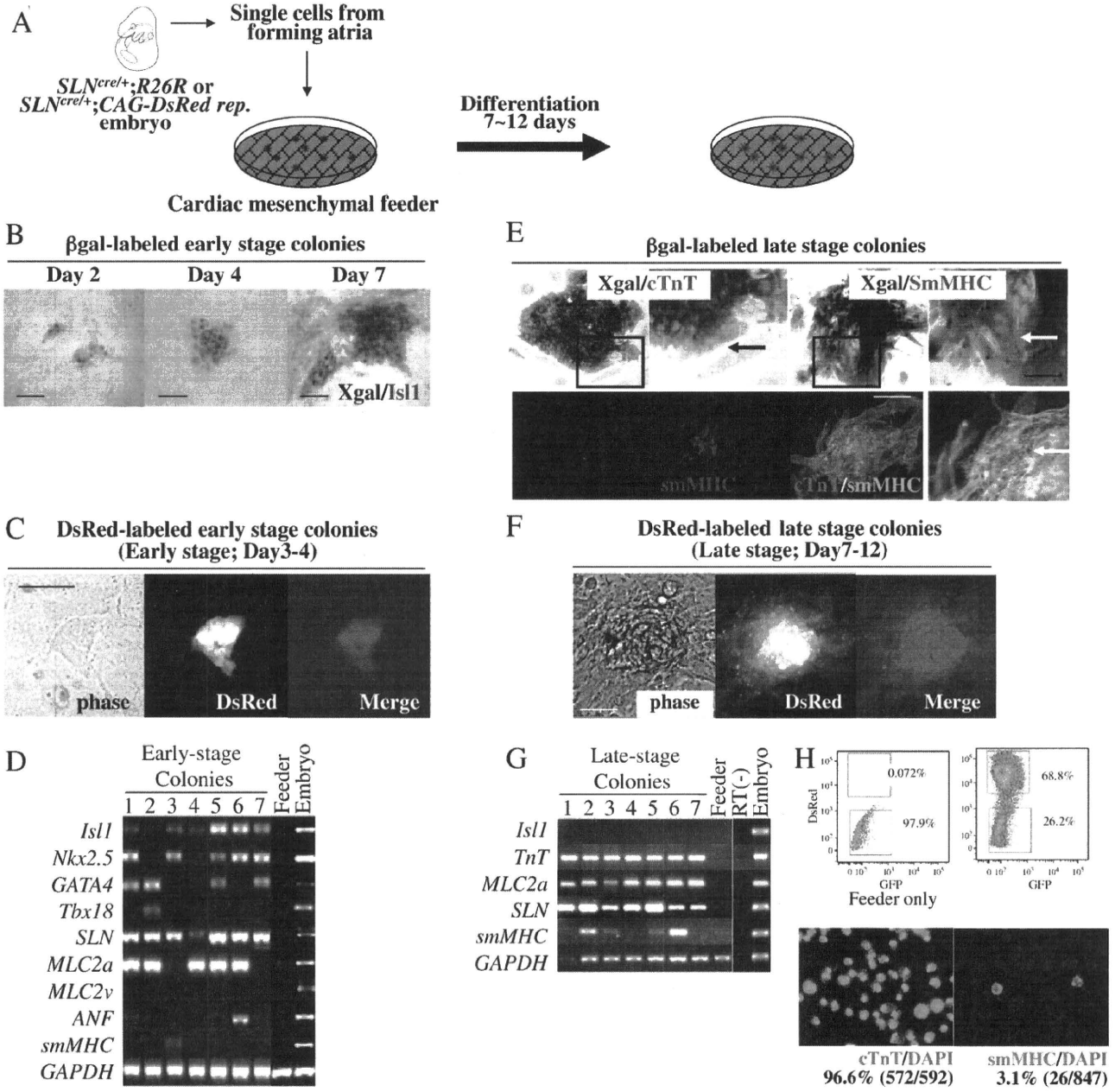

Fig. 5. Isl1$^+$/SLN$^+$ cells clonally give rise to cardiac and smooth muscle cells. (A) The forming atria of E9.5 *SLN*$^{cre/+}$ × *R26R* or *SLN*$^{cre/+}$ × *CAG-DsRed reporter* embryos are dissected and dissociated with collagenase. βGal- or DsRed-labeled atrial progenitors are cultured on cardiac mesenchymal feeders at clonal density. The dissociated atrial tissues are grown for 7–12 days and then examined for cardiac and smooth muscle marker expression. (B) Colonies are stained for Isl1 at early stages (2, 4 and 7 days after isolation). βGal-labeled atrial cells maintain Isl1 expression up to 7 days on a cardiac mesenchymal feeder layer. Scale bar = 50 μm. (C) DsRed-labeled atrial progenitor colonies grown for 4 days on feeders. (D) DsRed-labeled atrial progenitors are manually picked up 4 days after isolation, and examined for marker expression by RT-PCR. Shown are 7 representative colonies. Most of the colonies expressed early cardiac markers (Isl1, Nkx2.5 and GATA4) and atrial markers (SLN and MLC2a). None of them are positive for MLC2v. At this stage, only few colonies expressed smMHC. (E) βGal-labeled atrial progenitors are differentiated for 7–12 days and stained for Xgal, cTnT and/or smMHC. Whereas most of the cells in Xgal-positive colonies were positive for cTnT, some in the periphery were negative (black arrow). These peripheral cells are co-stained with smMHC (white arrows). Lower panels show cTnT/smMHC immunofluorescent staining of a representative colony, indicating that these two cell types differentiate from a single cell (white arrow). (F) DsRed-labeled atrial colonies grown for 12 days on feeders. (G) Expression profile of atrial colonies. After 7–12 days (late stage) on feeders, colonies were picked up and examined for marker expression. RT-PCR revealed that Isl1 is already downregulated at this stage but SLN and MLC2a are still positive. Importantly, smMHC becomes positive in more than half of the colonies. (H) *Ex vivo* quantification of the percentage of smooth muscle cells derived from atrial lineage. After 7–12 days (late stage) on feeders, DsRed-labeled atrial colonies were FACS-sorted, attached on glass slides by cytospin, and stained for cTnT (left bottom panel) or smMHC (right bottom panel). Note that 3.1% of the progeny of atrial colonies were smooth muscle cells, while 96.6% were cardiomyocytes.

components of the posterior region of the secondary heart field [32], and retain proliferative activity [33] and bipotency until later stages of cardiogenesis, which apparently relates to their generation of the myocardial/smooth muscle sleeves that serve as the junctional boundary to connect the great vessels and the cardiac chambers into a functional syncytium. Interestingly, there are several diseases of the atrium and inflow tract, including a common form of congenital heart disease where the pulmonary venous inflow tract is ectopic or absent, and atrial fibrillation that relates to a reemergence of ectopic electrical activity in the pulmonary veins. The finding of bipotent

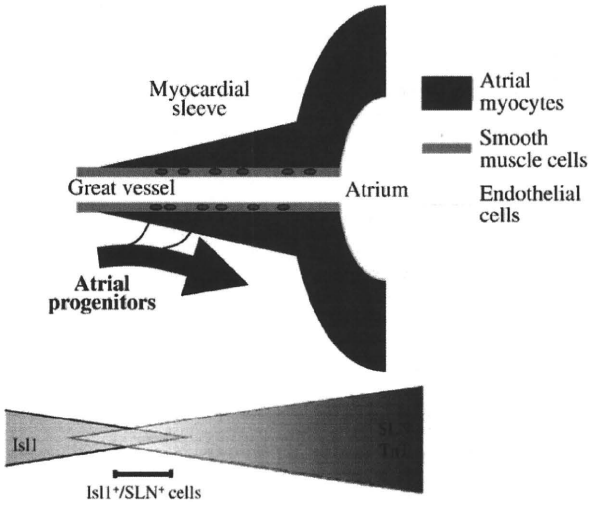

Fig. 6. A model for the migration of atrial progenitors. During the migration from the splanchnic mesoderm, Isl1-progentiors in the pSHF gradually lose Isl1 expression and start to express atrial specific markers including SLN. The Isl1$^+$/SLN$^+$ cells represent a transient cell population that is already committed to the atrial lineage, but still maintain proliferative and migratory activities. Isl1$^+$/SLN$^+$ cells mainly contribute to atrial myocardium, but some contribute to smooth muscle cells in the cardiac inflow tract. This smooth muscle competency is gradually lost during the migration and maturation.

Isl1$^+$/SLN$^+$ cells suggests the possibility that some of atrial diseases might arise from dys-regulation of the bipotency in atrial lineages.

The Isl1$^+$/SLN$^+$ atrial progenitor population includes at least three populations; working atrial myocytes, Nkx2.5$^-$/Tbx18$^+$ cardiac progenitors in the sinus venosus and mediastinal myocardium in the dorsal mesocardium [16,23,24,33–35]. These three populations derive from Isl1$^+$ posterior SHF progenitors and eventually acquire SLN expression, although our experiments cannot tell which population display smooth muscle competency. Discovery of earlier and later markers will help establish the lineage tree of the posterior SHF/venous pole population.

4.2. Lineage proximity of cardiac and smooth muscle cells

Smooth muscle cells appear to be recruited locally from a wide range of mesodermal tissues and differentiate in response to specific local signals. Our data suggest that during the migration from the posterior part of the SHF, Isl1$^+$/SLN$^+$ cells mainly contribute to mature atrial myocytes, but some cells escape from the cardiac lineage and give rise to the smooth muscle cells in the inflow tract (Fig. 6). Given that SLN is a relatively late marker of the atrial lineage, it is not unexpected that SLN$^+$ cells contribute only to 5–10% of the inflow smooth muscle cells. It is rather significant in that atrial cells give rise to smooth muscle cells *in vivo* even after the expression of SLN gene, which is involved in atrial specific contractile function [17,18].

It has been known that cardiac cells can transdifferentiate into smooth muscle cells even at the postnatal stage at low frequency upon certain culture conditions. However, little is known as to whether it is a dedifferentiation–redifferentiation process or a direct transition from differentiated cardiomyocyte to differentiated smooth muscle cell. Wu et al. reported that Nkx2.5-positive cardiac progenitors downregulate Nkx2.5 before committing to smooth muscle lineage [3]. Since Nkx2.5 is also expressed in atrial lineage, it is likely that atrial cells shut of cardiac transcriptional program in order to give rise to smooth muscle cells. Although our study cannot give a clear answer to this question, it raises the possibility that the smooth muscle competency of the postnatal myocytes may be a trace of the developmental potential of the embryonic cardiac progenitors and myocytes.

A fundamental question relates to how the smooth muscle differentiation of cardiac progenitors serves to coordinate the morphogenesis of the atrial chamber and great vessels. An interesting speculation is that the smooth muscle competency of the atrial cells is required to anchor the great veins to the atrial chambers. Malconnection of myocardium and vascular walls causes various types of congenital and adult heart diseases including anomalous pulmonary venous return and cor triatriatum [36]. In the aging and/or diseased hearts, the junctions between pulmonary veins and left atrium are highly arrhythmogenic and can be the foci of atrial fibrillation, one of the major causes of thromboembolic stroke [37–41]. Likewise, the heart-vessel junction at the arterial pole of the heart is often affected by various congenital malformations and acquired diseases including DeBakey Type I and II aortic dissection. It would be of great interest to analyze the pathogenesis of these congenital and acquired heart diseases from the viewpoint of progenitor cell plasticity.

Disclosures

None declared.

Acknowledgments

This work is supported by NIH, Jean Le Ducq foundation, Harvard Stem Cell Institute, Massachusetts General Hospital, UCLA, and Eli and Edythe Broad Center of Regenerative Medicine and Stem Cell Research. We thank Marianne Cilluffo at the Electron Microscopic Lab in Brain Research Institute, UCLA.

Appendix A. Supplementary data

Supplementary data to this article can be found online at doi:10.1016/j.yjmcc.2010.10.009.

References

[1] Kattman SJ, Huber TL, Keller GM. Multipotent flk-1$^+$ cardiovascular progenitor cells give rise to the cardiomyocyte, endothelial, and vascular smooth muscle lineages. Dev Cell 2006;11:723–32.
[2] Moretti A, Caron L, Nakano A, Lam JT, Bernshausen A, Chen Y, et al. Multipotent embryonic isl1$^+$ progenitor cells lead to cardiac, smooth muscle, and endothelial cell diversification. Cell 2006;127:1151–65.
[3] Wu SM, Fujiwara Y, Cibulsky SM, Clapham DE, Lien CL, Schultheiss TM, et al. Developmental origin of a bipotential myocardial and smooth muscle cell precursor in the mammalian heart. Cell 2006;127:1137–50.
[4] Yang L, Soonpaa MH, Adler ED, Roepke TK, Kattman SJ, Kennedy M, et al. Human cardiovascular progenitor cells develop from a KDR$^+$ embryonic-stem-cell-derived population. Nature 2008;453:524–8.
[5] Garry DJ, Olson EN. A common progenitor at the heart of development. Cell 2006;127:1101–4.
[6] Kattman SJ, Adler ED, Keller GM. Specification of multipotential cardiovascular progenitor cells during embryonic stem cell differentiation and embryonic development. Trends Cardiovasc Med 2007;17:240–6.
[7] Martin-Puig S, Wang Z, Chien KR. Lives of a heart cell: tracing the origins of cardiac progenitors. Cell Stem Cell 2008;2:320–31.
[8] Cai CL, Liang X, Shi Y, Chu PH, Pfaff SL, Chen J, et al. Isl1 identifies a cardiac progenitor population that proliferates prior to differentiation and contributes a majority of cells to the heart. Dev Cell 2003;5:877–89.
[9] Laugwitz KL, Moretti A, Caron L, Nakano A, Chien KR. Islet1 cardiovascular progenitors: a single source for heart lineages? Development 2008;135:193–205.
[10] Kelly RG, Brown NA, Buckingham ME. The arterial pole of the mouse heart forms from Fgf10-expressing cells in pharyngeal mesoderm. Dev Cell 2001;1:435–40.
[11] Mjaatvedt CH, Nakaoka T, Moreno-Rodriguez R, Norris RA, Kern MJ, Eisenberg CA, et al. The outflow tract of the heart is recruited from a novel heart-forming field. Dev Biol 2001;238:97–109.
[12] Waldo KL, Kumiski DH, Wallis KT, Stadt HA, Hutson MR, Platt DH, et al. Conotruncal myocardium arises from a secondary heart field. Development 2001;128:3179–88.
[13] Dodou E, Verzi MP, Anderson JP, Xu SM, Black BL. Mef2c is a direct transcriptional target of ISL1 and GATA factors in the anterior heart field during mouse embryonic development. Development 2004;131:3931–42.
[14] Waldo KL, Hutson MR, Ward CC, Zdanowicz M, Stadt HA, Kumiski D, et al. Secondary heart field contributes myocardium and smooth muscle to the arterial pole of the developing heart. Dev Biol 2005;281:78–90.

[15] Sun Y, Liang X, Najafi N, Cass M, Lin L, Cai CL, et al. Islet 1 is expressed in distinct cardiovascular lineages, including pacemaker and coronary vascular cells. Dev Biol 2007;304:286–96.
[16] Galli D, Dominguez JN, Zaffran S, Munk A, Brown NA, Buckingham ME. Atrial myocardium derives from the posterior region of the second heart field, which acquires left–right identity as Pitx2c is expressed. Development 2008;135:1157–67.
[17] Odermatt A, Taschner PE, Scherer SW, Beatty B, Khanna VK, Cornblath DR, et al. Characterization of the gene encoding human sarcolipin (SLN), a proteolipid associated with SERCA1: absence of structural mutations in five patients with Brody disease. Genomics 1997;45:541–53.
[18] Minamisawa S, Wang Y, Chen J, Ishikawa Y, Chien KR, Matsuoka R. Atrial chamber-specific expression of sarcolipin is regulated during development and hypertrophic remodeling. J Biol Chem 2003;278:9570–5.
[19] Babu GJ, Bhupathy P, Carnes CA, Billman GE, Periasamy M. Differential expression of sarcolipin protein during muscle development and cardiac pathophysiology. J Mol Cell Cardiol 2007;43:215–22.
[20] Xu H, Chen L, Baldini A. *In vivo* genetic ablation of the periotic mesoderm affects cell proliferation survival and differentiation in the cochlea. Dev Biol 2007;310:329–40.
[21] Soriano P. Generalized lacZ expression with the ROSA26 Cre reporter strain. Nat Genet 1999;21:70–1.
[22] Vintersten K, Monetti C, Gertsenstein M, Zhang P, Laszlo L, Biechele S, et al. Mouse in red: red fluorescent protein expression in mouse ES cells, embryos, and adult animals. Genesis 2004;40:241–6.
[23] Soufan AT, van den Hoff MJ, Ruijter JM, de Boer PA, Hagoort J, Webb S, et al. Reconstruction of the patterns of gene expression in the developing mouse heart reveals an architectural arrangement that facilitates the understanding of atrial malformations and arrhythmias. Circ Res 2004;95:1207–15.
[24] Anderson RH, Brown NA, Moorman AF. Development and structures of the venous pole of the heart. Dev Dyn 2006;235:2–9.
[25] Mommersteeg MT, Soufan AT, de Lange FJ, van den Hoff MJ, Anderson RH, Christoffels VM, et al. Two distinct pools of mesenchyme contribute to the development of the atrial septum. Circ Res 2006;99:351–3.
[26] Moorman AF, Christoffels VM, Anderson RH, van den Hoff MJ. The heart-forming fields: one or multiple? Philos Trans R Soc Lond B Biol Sci 2007;362:1257–65.
[27] Snarr BS, O'Neal JL, Chintalapudi MR, Wirrig EE, Phelps AL, Kubalak SW, et al. Isl1 expression at the venous pole identifies a novel role for the second heart field in cardiac development. Circ Res 2007;101:971–4.
[28] Snarr BS, Wirrig EE, Phelps AL, Trusk TC, Wessels A. A spatiotemporal evaluation of the contribution of the dorsal mesenchymal protrusion to cardiac development. Dev Dyn 2007;236:1287–94.
[29] Kruithof BP, van den Hoff MJ, Wessels A, Moorman AF. Cardiac muscle cell formation after development of the linear heart tube. Dev Dyn 2003;227:1–13.
[30] Bu L, Jiang X, Martin-Puig S, Caron L, Zhu S, Shao Y, et al. Human ISL1 heart progenitors generate diverse multipotent cardiovascular cell lineages. Nature 2009;460:113–7.
[31] Dyer LA, Kirby ML. The role of secondary heart field in cardiac development. Dev Biol 2009;336:137–44.
[32] Buckingham M, Meilhac S, Zaffran S. Building the mammalian heart from two sources of myocardial cells. Nat Rev Genet 2005;6:826–35.
[33] Soufan AT, van den Berg G, Ruijter JM, de Boer PA, van den Hoff MJ, Moorman AF. Regionalized sequence of myocardial cell growth and proliferation characterizes early chamber formation. Circ Res 2006;99:545–52.
[34] Christoffels VM, Mommersteeg MT, Trowe MO, Prall OW, de Gier-de Vries C, Soufan AT, et al. Formation of the venous pole of the heart from an Nkx2-5-negative precursor population requires Tbx18. Circ Res 2006;98:1555–63.
[35] Mommersteeg MT, Brown NA, Prall OW, de Gier-de Vries C, Harvey RP, Moorman AF, et al. Pitx2c and Nkx2-5 are required for the formation and identity of the pulmonary myocardium. Circ Res 2007;101:902–9.
[36] Nakano A, Nakano H, Chien KR. Multipotent islet-1 cardiovascular progenitors in development and disease. Cold Spring Harb Symp Quant Biol 2008;73:297–306.
[37] Jais P, Haissaguerre M, Shah DC, Chouairi S, Gencel L, Hocini M, et al. A focal source of atrial fibrillation treated by discrete radiofrequency ablation. Circulation 1997;95:572–6.
[38] Haissaguerre M, Jais P, Shah DC, Takahashi A, Hocini M, Quiniou G, et al. Spontaneous initiation of atrial fibrillation by ectopic beats originating in the pulmonary veins. N Engl J Med 1998;339:659–66.
[39] Haissaguerre M, Shah DC, Jais P, Hocini M, Yamane T, Deisenhofer I, et al. Electrophysiological breakthroughs from the left atrium to the pulmonary veins. Circulation 2000;102:2463–5.
[40] Chen PS, Chou CC, Tan AY, Zhou S, Fishbein MC, Hwang C, et al. The mechanisms of atrial fibrillation. J Cardiovasc Electrophysiol 2006;17(Suppl 3):S2–7.
[41] Ocorr K, Reeves NL, Wessells RJ, Fink M, Chen HS, Akasaka T, et al. KCNQ potassium channel mutations cause cardiac arrhythmias in Drosophila that mimic the effects of aging. Proc Natl Acad Sci U S A 2007;104:3943–8.

European Journal of Pharmacology 649 (2010) 263–267

Contents lists available at ScienceDirect

European Journal of Pharmacology

journal homepage: www.elsevier.com/locate/ejphar

Cardiovascular Pharmacology

Effects of *S*(+)-efonidipine on the rabbit sinus node action potential and calcium channel subunits $Ca_V1.2$, $Ca_V1.3$ and $Ca_V3.1$

Hikaru Tanaka [a,*], Iyuki Namekata [a], Toru Ogawa [a], Yayoi Tsuneoka [a], Chisa Komikado [a], Akira Takahara [a], Naoko Iida-Tanaka [a,b], Hiroko Izumi-Nakaseko [c], Hiromichi Tsuru [c], Satomi Adachi-Akahane [c]

[a] Department of Pharmacology, Toho University Faculty of Pharmaceutical Sciences, Funabashi, Chiba 274-8510, Japan
[b] Department of Food Science, Faculty of Home Economics, Otsuma Woman's University, Chiyoda-ku, Tokyo 102-8357, Japan
[c] Department of Pharmacology, Toho University Faculty of Medicine, Ohta-ku, Tokyo 143-8540, Japan

ARTICLE INFO

Article history:
Received 25 December 2009
Received in revised form 10 August 2010
Accepted 7 September 2010
Available online 19 September 2010

Keywords:
S(+)-efonidipine
Sinus node
Calcium channel
$Ca_V1.3$

ABSTRACT

The effect of *S*(+)-efonidipine on sinus node action potential and calcium channel α-subunits was examined. The slope of the phase 4 depolarization of isolated rabbit sinus node tissue was significantly reduced by *S*(+)-efonidipine (1 μM), slightly reduced by nifedipine (1 μM), but was not affected by *R*(−)-efonidipine. *S*(+)-efonidipine (1 μM), inhibited the expressed $Ca_V1.2$, $Ca_V1.3$ and $Ca_V3.1$ channel currents by 75.7%, 75.3% and 94.0%, nifedipine 84.0%, 43.2% and 14.9%, and *R*(−)-efonidipine 30.0%, 19.6% and 92.8%, respectively. Thus, the prolongation of the phase 4 depolarization of the rabbit sinus node by *S*(+)-efonidipine may be explained by blockade of the $Ca_V1.3$ channel current.

1. Introduction

Efonidipine is an antihypertensive and antianginal drug with dihydropyridine structure, which was developed as an antihypertensive agent with slow onset and long duration of action. It has excellent clinical profiles such as moderate reduction of heart rate (Masuda and Tanaka, 1994; Shimizu et al, 2001; Tanaka and Shigenobu, 2002; Tanaka et al., 2007; Morimoto et al., 2009; Ohashi et al., 2009). Studies with rabbit isolated sinus node preparations revealed that efonidipine prolongs the phase 4 (diastolic) depolarization leading to reduction of heart rate, which could be explained through its dual blocking effect on L-type and T-type Ca^{2+} channels (Masumiya et al., 1997, 1998; Tanaka and Shigenobu, 2005). Recently, however, the *R*(−)-enantiomer of efonidipine, which selectively blocks the T-type Ca^{2+} channel (Furukawa et al., 2004; Tanaka et al., 2004), was shown to have no prolonging effect on the phase 4 depolarization of the rabbit isolated sinus node (Tanaka et al., 2008). This observation raised the possibility that the prolonging effect of efonidipine on the phase 4 depolarization of this preparation originates in the *S*(+)-enantiomer, and that mechanisms other than T-type Ca^{2+} channel inhibition might be involved. Concerning L-type Ca^{2+} channels, an α-subunit encoded by $Ca_V1.3$, which activates at more negative voltage than that encoded by $Ca_V1.2$, has been postulated to contribute to the phase 4 depolarization of the sinus node based on experiments with $Ca_V1.3$ deficient mice (Platzer et al., 2000; Koschak et al., 2001; Zhang et al., 2002; Mangoni et al., 2003; Ono and Iijima, 2005).

In the present study, we examined the effects of *S*(+)-efonidipine on the rabbit sinus node action potential to clarify whether the prolongation of phase 4 depolarization by racemic efonidipine can be ascribed to the *S*(+)-enantiomer. Further, to obtain information on its mechanism of action, we examined the effects of *S*(+)-efonidipine on Ca^{2+} channel α-subunits $Ca_V1.2$, $Ca_V1.3$ and $Ca_V3.1$, and compared them with the effects of nifedipine and *R*(−)-efonidipine.

2. Materials and methods

2.1. Action potential measurements

The present study was approved by the Ethics Committee of Toho University, and was conducted in accordance with the Guiding "Principles for the Care and Use of Laboratory Animals Approved by The Japanese Pharmacological Society". Standard glass microelectrode experiments were performed with isolated rabbit sinus node tissue as in our previous study (Masumiya et al., 1997; Tanaka et al., 2008). Male rabbits weighing 2 to 3 kg were anesthetized with sodium pentobarbital (30 mg/kg) and the hearts were quickly isolated. Tissue including the sinus node were cut perpendicularly to the crista terminalis into strips

* Corresponding author. Department of Pharmacology, Toho University Faculty of Pharmaceutical Sciences, Miyama 2-2-1, Funabashi, Chiba 274-8510, Japan. Tel.: +81 474722092; fax: +81 474722113.
E-mail address: htanaka@phar.toho-u.ac.jp (H. Tanaka).

0014-2999/$ – see front matter © 2010 Elsevier B.V. All rights reserved.
doi:10.1016/j.ejphar.2010.09.014

of about 1 × 3 mm. Preparations were pinned down horizontally on a silicon block in a 20 ml organ bath containing physiological salt solution of the following composition (mM concentration): NaCl, 118.4; KCl, 4.7; $CaCl_2$, 2.5; $MgSO_4$, 1.2; KH_2PO_4, 1.2; $NaHCO_3$, 24.9; and glucose, 11.1 (gassed with 95% O_2–5% CO_2, pH 7.4). The temperature of the organ bath was maintained at 36 °C. Penetration of microelectrodes filled with 3 M KCl (resistance, 20 to 50 MΩ) was made into dominant pacemaker cells. The output of the microelectrode amplifier (MEZ-8201, Nihon Kohden, Tokyo, Japan) was fed into an AD converter (Analog Pro, Canopus, Kobe, Japan) attached to a computer (PC 9801 FA2, NEC, Tokyo, Japan) for the analyses. The parameters measured were cycle length, maximum diastolic potential, slope of the diastolic depolarization (slope), threshold potential, maximum rate of rise of the upstroke of the action potential (maximum rate of rise), overshoot, and duration at 50% repolarization. The effect of efonidipine on the action potential in myocardial tissue preparations is known to be slow in onset and requires higher concentrations than its effects on calcium currents in single cells (Okuyama et al., 1994; Masuda et al., 1995; Tanaka et al., 1996; Masumiya et al., 1998). To measure the effect of drugs on the action potential accurately, we used a single relatively high concentration of drugs (1 μM). The exposure time was 2 min for nifedipine but was 30 min for efonidipine, which required longer time for its effect to reach steady state. For the interpretation of results, the effect of the two enantiomers of efonidipine might have to be compared with their effects on the calcium currents at lower concentrations.

2.2. Expression and analysis of $Ca_V1.2$ and $Ca_V1.3$

Expression of calcium channel α-subunits $Ca_V1.2$, $Ca_V1.3$ in BHK6 cells and current measurement were performed as previously described (Yamaguchi et al., 2000). The cDNA for $Ca_V1.2$ and $Ca_V1.3$ were generously provided by Dr. Snutch, T.P. (British Columbia University, Canada) and Striessnig, J. (University of Innsbruck, Austria), respectively. The full length cDNAs for $Ca_V1.2$ and $Ca_V1.3$ were introduced into BHK6 cells expressing the calcium channel β_{1a} and α_2/δ subunits. We confirmed that $Ca_V1.3$ activated at more negative voltages compared to $Ca_V1.2$ by approximately 20 mV, as has been reported (Koschak et al., 2001). Therefore, inward currents through $Ca_V1.2$ and $Ca_V1.3$ channels were elicited by 100 ms depolarizing voltage clamp pulses from −80 mV to 10 mV and −10 mV, respectively. The extracellular solution was of the following composition (mM concentration): NaCl, 137.0; KCl, 5.4; $BaCl_2$, 10; $MgCl_2$, 1; glucose, 10; tetrodotoxin 0.0001; HEPES, 10 (pH 7.4) and the pipette solution was of the following composition (mM concentration): cesium methanesulfonate, 120; tetraethylammoniumCl, 20; EGTA, 14; ATP-Mg, 5; Na_2GTP, 0.2;Na_2 creatine phosphate, 5; HEPES, 10 (pH 7.3). The charge carrier for the calcium channel currents was Ba^{2+} instead of Ca^{2+}. The output of the patch clamp amplifier (HEKA Elektonik, Lambrecht Germany) was digitalized with an AD converter (Digidata 1322A, Axon Instruments Inc., Foster City USA) and analyzed (pClamp-9 software, Axon Instruments Inc., Foster City USA). The exposure time of the drugs on the calcium channel currents was 10 min, during which the current rundown was less than 5%.

2.3. Expression and analysis of $Ca_V3.1$

The full length cDNA for $Ca_V3.1$ was obtained by polymerase chain reaction from a mouse heart cDNA library (Takara Bio Co., Ltd., Kyoto, Japan) according to the published mouse cDNA sequence (Klugbauer et al., 1999; GenBank accession number AJ012569), and inserted into the mammalian expression vector pIRESneo3 (Takara Bio Co., Ltd., Kyoto, Japan). This vector was introduced into HEK293 cells with lipofectamine 2000 (Invitrogen, Carlsbad CA, USA) and stable transformants were obtained by clone culture in the presence of 500 μM G418. Inward currents through the $Ca_V3.1$ channels were elicited by 200 ms depolarizing voltage clamp pulses from −80 mV to −30 mV, as described previously (Tanaka et al., 2008). The extracellular solution was of the following composition (mM concentration): NaCl, 143.0; KCl, 5.4; $CaCl_2$, 1.8; $MgCl_2$, 1.0; KH_2PO_4, 0.33; HEPES, 5.0; and glucose, 5.5 (pH 7.4). The pipette solution was of the following composition (mM concentration): CsCl, 80; CsOH, 40; ATP-Mg, 5; EGTA, 10; and HEPES, 10 (pH 7.2). The patch clamp amplifier used was Axopatch 1D (Axon Instruments Inc., Foster City CA, USA) and the AD converter was Digidata 1200 (Axon Instruments Inc., Foster City CA, USA). The exposure time of the drugs on the calcium channel currents was 10 min, during which the current rundown was less than 5%.

2.4. Data analysis and statistics

Data were presented as mean ± standard errors (S.E.M.). Statistical significance between means was evaluated by the paired t-test or by one-way analysis of variance followed by Dunnett's test for multiple comparisons. P values less than 0.05 were considered significant.

2.5. Drugs and chemicals

The enantiomers of efonidipine {5-(5,5-Dimethyl-1,3,2-dioxaphosphorinan-2-yl)-1,4-dihydro-2,6-dimethyl-4-(3-nitrophenyl)-3-pyridinecarboxylic acid 2-[phenyl(phenylmethyl)amino]ethyl ester} were provided by Nissan Chemical Industries, Ltd. (Tokyo, Japan), and nifedipine was purchased from Wako Pure Chemical Industries, Ltd. (Osaka, Japan). The drugs were dissolved in DMSO and small aliquots were applied to the extracellular solution; the final concentration of DMSO was 0.05%. All other chemicals were commercial products of the highest available quality.

3. Results

3.1. Effect of S(+)-efonidipine, nifedipine and R(−)-efonidipine on sinus node action potential

The effect of S(+)-efonidipine on sinus node action potential was examined and compared with those of nifedipine and R(−)-efonidipine (Fig. 1; Table 1). S(+)-Efonidipine (1 μM) significantly reduced the slope of phase 4 and phase 0 depolarization. Nifedipine (1 μM) also significantly reduced the slope of phase 0 depolarization but only slightly reduced the slope of phase 4 depolarization. R(−)-efonidipine (1 μM) had no significant effect on these parameters. S(+)-efonidipine and nifedipine prolonged the cycle length and shifted the maximum diastolic potential and the threshold potential towards depolarized potentials but such effects were not observed with R(−)-efonidipine.

3.2. Effect of S(+)-efonidipine on calcium channel currents

The effect of S(+)-efonidipine on calcium channel α-subunits $Ca_V1.2$, $Ca_V1.3$ and $Ca_V3.1$ were compared with those of nifedipine and R(−)-efonidipine. S(+)-Efonidipine inhibited the expressed $Ca_V1.2$, $Ca_V1.3$ and $Ca_V3.1$ channel currents with similar potency (Fig. 2Aabc; 2Ba). The effect was concentration-dependent and the percent inhibition of $Ca_V1.2$, $Ca_V1.3$ and $Ca_V3.1$ currents by 1 μM S(+)-efonidipine was 75.7%, 75.3% and 94.0%, respectively, and the EC_{50} value was 0.46 μM, 0.32 μM and 0.11 μM, respectively.

3.3. Effect of nifedipine on calcium channel currents

Nifedipine inhibited the expressed $Ca_V1.2$, $Ca_V1.3$ and $Ca_V3.1$ channel currents; the effect was concentration-dependent and the potency order was CaV1.2>$Ca_V1.3$>$Ca_V3.1$ (Fig. 2Adef; 2Bb). Percent inhibition of $Ca_V1.2$, $Ca_V1.3$ and $Ca_V3.1$ currents by 1 μM nifedipine was 84.0%, 43.2% and 14.9%, respectively, and the EC_{50} value for the $Ca_V1.2$ and $Ca_V1.3$ channel currents was 0.19 μM and 2.82 μM, respectively.

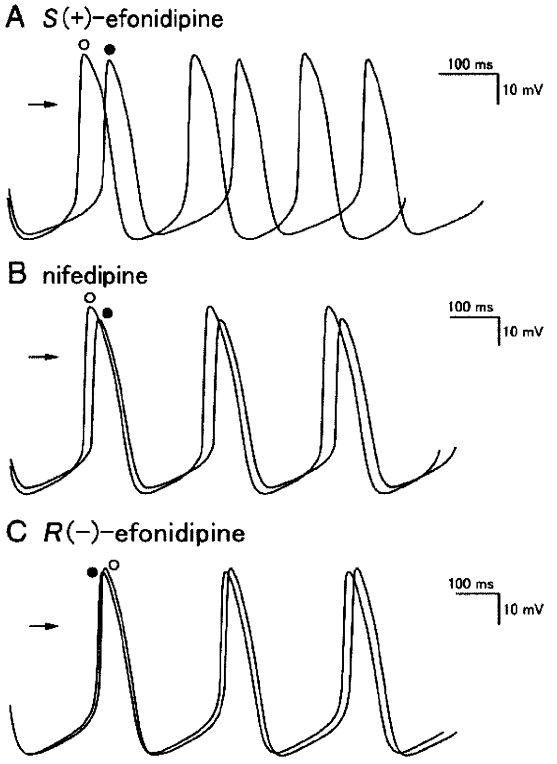

Fig. 1. Effects of *S*(+)-efonidipine, nifedipine and *R*(−)-efonidipine on rabbit sinus node action potential. Typical recordings before (open circles) and after (closed circles) the addition of 1 μM *S*(+)-efonidipine (A), 1 μM nifedipine (B) and 1 μM *R*(−)-efonidipine (C). Arrows indicate 0 mV level.

3.4. Effect of *R*(−)-efonidipine on calcium channel currents

R(−)-Efonidipine inhibited the expressed $Ca_V1.2$, $Ca_V1.3$ and $Ca_V3.1$ channel currents; the effect was concentration-dependent and the potency order was $Ca_V3.1 > Ca_V1.2 = Ca_V1.3$ (Fig. 2Bc). Percent inhibition of $Ca_V1.2$, $Ca_V1.3$ and $Ca_V3.1$ currents by 1 μM *R*(−)-efonidipine was 30.0%, 19.6% and 92.8%, respectively, and the EC_{50} value for the $Ca_V3.1$ channel current was 0.20 μM.

4. Discussion

4.1. Prolongation of the phase 4 depolarization of sinus node action potential

The main objective of the present study was to determine whether the effect of efonidipine to prolong the phase 4 depolarization of the sinus node originates in the *S*(+)-enantiomer. In the rabbit sinus node, *S*(+)-efonidipine significantly reduced the slope of phase 4 depolarization (Fig. 1A), which was the same as the effect of racemic efonidipine (Masumiya et al., 1997); such effect was not observed with *R*(−)-efonidipine (Fig. 1C). These results clearly indicate that prolongation of the phase 4 depolarization of rabbit sinus node is caused by the *S*(+)-enantiomer. Thus, clarification of the mechanism of action of *S*(+)-efonidipine may lead to a new understanding of pacemaker mechanisms. *S*(+)-efonidipine and nifedipine caused a slight positive shift of the maximum diastolic potential. As the inhibitory effect of efonidipine and nifedipine on the inwardly rectifying and delayed rectifying potassium currents are minimal (Masumiya et al., 1998), and efonidipine had no effect on the hyperpolarization-activated inward current (unpublished observation), effects on other ionic currents and/or indirect mechanisms may be involved.

4.2. Possible mechanism for the prolongation of phase 4 depolarization

S(+)-efonidipine blocked all three calcium channel α subunits $Ca_V1.2$, $Ca_V1.3$ and $Ca_V3.1$ with similar potency (Fig. 2Ba), EC_{50} values being 0.46, 0.32 and 0.11 (μM), respectively. To obtain information on the mechanism of action for the prolongation of phase 4 depolarization by *S*(+)-efonidipine, the effects were compared with those of nifedipine and *R*(−)-efonidipine. Nifedipine, which blocked the $Ca_V1.2$ and $Ca_V1.3$ channel currents with EC_{50} values of 0.19 and 2.28 (μM), respectively (Fig. 2Bb), produced a less prominent prolongation of phase 4 depolarization (Fig. 1B). *R*(−)-efonidipine, which was selective for the $Ca_V3.1$ channel (Fig. 2Bc), had no prolonging effect on phase 4 depolarization (Fig. 1C). This parallelism of potency of the three compounds to block the $Ca_V1.3$ channel and to prolong the phase 4 depolarization suggests a causal relationship; the $Ca_V1.3$ channel current contributes to phase 4 depolarization. The $Ca_V1.3$ channel may be a novel target molecule for the development of bradycardiac agents. The activation threshold for the $Ca_V1.2$ channel is

Table 1
Action potential parameters before and after application of *S*(+)-efonidipine, nifedipine, *R*(−)-efonidipine and their vehicle.

	S(+)-efonidipine (n=5)		nifedipine (n=5)		*R*(−)-efonidipine (n=5)		vehicle (DMSO) (n=5)	
	before	after	before	after	before	after	before	after
Cycle length (ms)	296±27	322±26[a] (26±7)[b]	304±15	314±15[a] (11±1)	325±37	318±33 (−7±5)	316±19	312±21 (−3±3)
Maximum diastolic potential (mV)	−60.5±0.3	−56.6±0.8[a] (4.0±0.8)	−61.0±2.0	−58.7±2.2[a] (2.4±0.4)	−59.8±0.8	−57.1±1.6 (2.7±1.5)	−59.6±3.0	−58.2±2.7 (1.4±0.6)
Slope (mV/s)	89.1±11.1	71.3±7.3[a] (−17.8±5.8)[b]	90.1±5.1	82.0±3.4 (−8.1±4.9)	79.8±12.1	78.3±13.1 (−1.5±1.9)	88.3±6.7	89.3±6.8 (1.0±1.0)
Threshold potential (mV)	−47.9±1.4	−43.2±0.8[a] (4.7±1.0)	−47.6±2.0	−45.8±1.8[a] (1.8±0.4)	−38.1±3.0	−36.4±2.4 (2.8±1.8)	−45.7±2.9	−44.0±2.7 (1.7±0.7)
Maximum rate of rise (V/s)	13.2±2.3	10.3±2.4[a] (−2.9±0.6)	14.2±2.7	11.2±1.9[a] (−2.9±0.9)	14.4±3.1	12.1±2.6 (−2.3±0.9)	10.7±1.6	9.7±1.5 (−1.0±0.6)
Overshoot (mV)	20.6±2.5	17.3±4.3 (−3.3±2.0)	17.7±2.2	14.4±2.3[a] (−3.3±0.3)	21.1±2.5	20.2±2.6 (−1.0±0.5)	22.0±1.5	22.5±1.7 (0.4±0.3)
Duration at 50% repolarization (ms)	60.6±3.5	56.5±4.1[a] (−4.2±0.8)[b]	67.1±6.0	62.5±5.7[a] (−4.6±0.8)[b]	69.5±2.7	68.1±2.9[a] (−1.4±0.4)	68.5±6.0	67.8±6.0 (−0.7±0.4)

Slope indicates the slope of the phase 4 depolarization and maximum rate of rise indicates the maximum slope of the action potential upstroke (phase 0). After: 30 min after the application of 1 μM *S*(+)-efonidipine and *R*(−)-efonidipine and vehicle (0.05% DMSO), 2 min after the application of 1 μM nifedipine. The changes in parameters are indicated in parenthesis.
[a] Significant difference from corresponding values before the application of drugs as evaluated by the paired t-test.
[b] Significant difference from corresponding changes after vehicle application as evaluated by Dunnett's test for multiple comparisons.

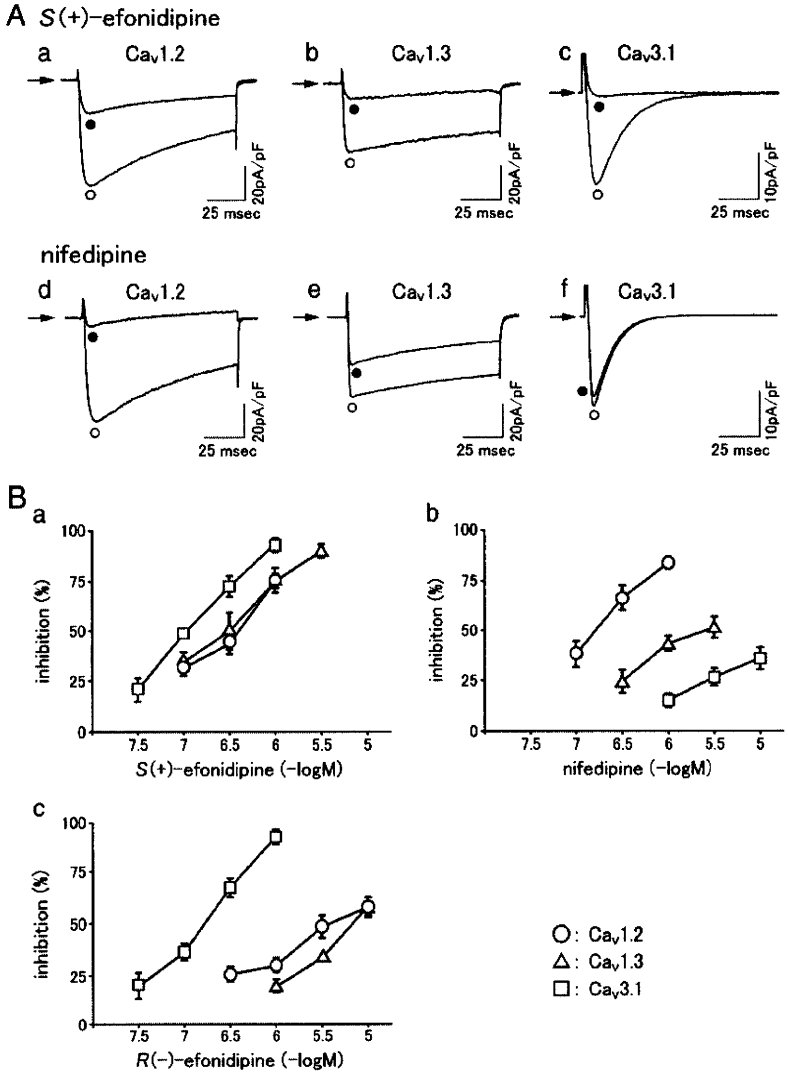

Fig. 2. Effects of *S*(+)-efonidipine, nifedipine and *R*(−)-efonidipine on calcium channel α-subunits $Ca_V1.2$, $Ca_V1.3$ and $Ca_V3.1$. A: Typical current recordings before (open circles) and after (closed circles) the addition of 1 μM *S*(+)-efonidipine on $Ca_V1.2$ (a), $Ca_V1.3$ (b) and $Ca_V3.1$ (c) channel currents and 1 μM nifedipine on $Ca_V1.2$ (d), $Ca_V1.3$ (e) and $Ca_V3.1$ (f) channel currents. Arrows indicate zero current level. B: Concentration–response relationship for the effects of *S*(+)-efonidipine (a), nifedipine (b) and *R*(−)-efonidipine (c) on calcium channel α-subunits $Ca_V1.2$ (circles), $Ca_V1.3$ (triangles) and $Ca_V3.1$ (squares). Symbols and vertical bars indicate the mean ± standard error of the mean from five to eight experiments.

about −30 mV (Koschak et al., 2001), which is more positive than the threshold potential (takeoff potential) of the sinus node action potential. Thus, the inhibitory effect of S(+)-efonidipine and nifedipine on the $Ca_V1.2$ channel current can be the cause of the decrease in maximum rate of rise, but not of the decreases in the slope and threshold potential (Table 1). Concerning the $Ca_V3.1$ channel current (T-type calcium current), we have previously reported that *R*(−)-efonidipine prolongs the phase 4 depolarization of the sinus node action potential in the mouse and guinea-pig but not in the rabbit (Tanaka et al., 2008). This agrees with the view that, under normal conditions, the T-type calcium current contributes to phase 4 depolarization in smaller animals such as the mouse and guinea-pig, but not in larger animals such as the rabbit and pig (Ono and Iijima, 2005).

4.3. Contribution of the $Ca_V1.3$ channel current to phase 4 depolarization

Contribution of the $Ca_V1.3$ channel current to the phase 4 depolarization of the sinus node action potential is consistent with the reported electrophysiological properties of the $Ca_V1.3$ channel. The $Ca_V1.3$ channel was reported to have an activation range of −50 mV to −10 mV, the voltage for 5% activation being −46 mV (Koschak et al., 2001). These values were about 20 mV negative than those for $Ca_V1.2$. This means that the $Ca_V1.3$ channel current can contribute to the phase 4 depolarization of the sinus node which occurs at −60 to −40 mV. This does not necessarily exclude the contribution of other membrane currents to phase 4 depolarization. In fact, the reduction of the slope by *S*(+)-efonidipine was partial which indicates that *S*(+)-efonidipine-insensitive mechanisms also contribute to the phase 4 depolarization of the rabbit sinus node.

5. Conclusion

The present results indicated that *S*(+)-efonidipine is responsible for the prolongation by racemic efonidipine of the phase 4 depolarization of the rabbit sinus node, and provided pharmacological evidence that the $Ca_V1.3$ channel current contributes to the phase 4 depolarization of the sinus node action potential.

Acknowledgments

This study was partly performed as a part of the project "Research on the molecular mechanisms of appearance of age-related diseases by failure of cell function control system, and their prevention and treatment" by the "Research Center for Aging and Age-Related Diseases" established in the Toho University Faculty of Pharmaceutical Sciences. This study was supported in part by Grants-in-Aid from the Ministry of Education, Culture, Sports, Science, and Technology of Japan to I.N (#22790262), A.T. (#21590602), and H.T.(#21590293) and by The Pharmacological Research Foundation, Tokyo. This study was supported in part by a research grant for collaborative research project in Toho University.

References

Furukawa, T., Miura, R., Honda, M., Kamiya, N., Mori, Y., Takeshita, S., Isshiki, T., Nukada, T., 2004. Identification of *R*-(−)-isomer of efonidipine as a selective blocker of T-type Ca^{2+} channels. Br. J. Pharmacol. 143, 1050–1057.

Klugbauer, N., Marais, E., Lacinova, L., Hofmann, F., 1999. A T-type calcium channel from mouse brain. Pflugers Arch. Eur. J. Physiol. 437, 710–715.

Koschak, A., Reimer, D., Huber, I., Grabner, M., Glossmann, H., Engel, J., Striessnig, J., 2001. α1D ($Ca_V1.3$) subunits can form L-type Ca^{2+} channels activating at negative voltages. J Biol Chem 276, 22100–22106.

Mangoni, M.E., Couette, B., Bourinet, E., Platzer, J., Reimer, D., Striessnig, J., Nargeot, J., 2003. Functional role of L-type $Ca_V1.3$ Ca^{2+} channels in cardiac pacemaker activity. Proc. Natl. Acad. Sci. USA 100, 5543–5548.

Masuda, Y., Tanaka, S., 1994. Efonidipine hydrochloride: a new calcium antagonist. Cardiovasc. Drug Rev. 12, 123–135.

Masuda, Y., Miyajima, M., Shudo, C., Tanaka, S., Shigenobu, K., Kasuya, Y., 1995. Cardiovascular selectivity of 1, 4-dihydropyridine derivatives, efonidipine (NZ-105), nicardipine and structure related compounds in isolated guinea-pig tissues. Gen. Pharmacol. 26, 339–345.

Masumiya, H., Tanaka, H., Shigenobu, K., 1997. Effects of Ca^{2+} channel antagonists on sinus node: prolongation of late phase 4 depolarization by efonidipine. Eur. J. Pharmacol. 335, 15–21.

Masumiya, H., Shijyuku, T., Tanaka, H., Shigenobu, K., 1998. Inhibition of myocardial T- and L-type Ca^{2+} currents by efonidipine: possible mechanism for its chronotropic effect. Eur. J. Pharmacol. 349, 351–357.

Morimoto, S., Jo, T., Maki, K., Iwasaka, T., 2009. Effects of efonidipine hydrochloride on heart rate and circulatory changes due to stress. Clin. Exp. Hypertens. 31, 83–91.

Ohashi, N., Mitamura, H., Ogawa, S., 2009. Development of newer calcium channel antagonists: therapeutic potential of efonidipine in preventing electrical remodeling during atrial fibrillation. Drugs 69, 21–30.

Okuyama, R., Adachi-Akahane, S., Nagao, T., 1994. Differential potentiation by depolarization of the effects of calcium antagonists on contraction and Ca^{2+} current in guinea-pig heart. Br. J. Pharmacol. 113, 451–456.

Ono, K., Iijima, T., 2005. Ionic and molecular basis of cardiac automaticity in mammalian heart. In: Mizukami, Y., Ohtsuka, T. (Eds.), Molecular mechanisms of heart diseases. Research SignPost, Trivandrum, pp. 1–22.

Platzer, J., Engel, J., Schrott-Fischer, A., Stephan, K., Bova, S., Chen, H., Zheng, H., Striessnig, J., 2000. Congenital deafness and sinoatrial node dysfunction in mice lacking class D L-type Ca^{2+} channels. Cell 102, 89–97.

Shimizu, M., Ogawa, K., Sasaki, H., Mizokami, T., Uehara, Y., Mochizuki, S., 2001. Effect of efonidipine hydrochloride, dihydropyridine Ca^{2+} antagonist with T-type Ca^{2+} channel blocking action, on heart rate. Ther. Res. 22, 883–889.

Tanaka, H., Shigenobu, K., 2002. Efonidipine hydrochloride: a dual blocker of L- and T-type Ca^{2+} channels. Cardiovasc. Drug Rev. 20, 81–92.

Tanaka, H., Shigenobu, K., 2005. Pathophysiological significance of T-type Ca^{2+} channels: T-type Ca^{2+} channels and drug development. J. Pharmacol. Sci. 99, 214–220.

Tanaka, H., Masumiya, H., Sekine, T., Shijuku, T., Sugahara, M., Taniguchi, H., Terada, M., Saito, W., Shigenobu, K., 1996. Myocardial and vascular effects of efonidipine in vitro as compared with nifedipine, verapamil and diltiazem. Gen. Pharmacol. 27, 451–454.

Tanaka, H., Komikado, C., Shimada, H., Takeda, K., Namekata, I., Kawanishi, T., Shigenobu, K., 2004. The *R*(−)-enantiomer of efonidipine blocks T-type but not L-type calcium current in guinea pig ventricular myocardium. J. Pharmacol. Sci. 96, 499–501.

Tanaka, H., Komikado, C., Namekata, I., Nakamura, H., Suzuki, M., Tsuneoka, Y., Shigenobu, K., Takahara, A., 2008. Species difference in the contribution of T-type calcium current to cardiac pacemaking as revealed by *R*(−)-efonidipine. J. Pharmacol. Sci. 107, 99–102.

Tanaka, T., Tsutamoto, T., Sakai, H., Fujii, M., Yamamoto, T., Horie, M., 2007. Comparison of the effects of efonidipine and amlodipine on aldosterone in patients with hypertension. Hypertens. Res. 30, 691–697.

Yamaguchi, S., Okamura, Y., Nagao, T., Adachi-Akahane, S., 2000. Serine residue in the IIIS5-S6 linker of the L-type Ca^{2+} channel α_{1c} subunit is the critical determinant of the action of dihydropyridine Ca^{2+} channel agonists. J. Biol. Chem. 275, 41504–41511.

Zhang, Z., Zu, Y., Song, H., Rodriguez, J., Tuteja, D., Namkung, Y., Shin, H., Chiamvimonvat, N., 2002. Functional roles of $Ca_V1.3$ ($\alpha 1_D$) calcium channel in sinoatrial nodes. Insight gained using gene-targeted null mutant mice. Circ. Res. 90, 981–987.

Effect of NIP-142 on Potassium Channel α-Subunits Kv1.5, Kv4.2 and Kv4.3, and Mouse Atrial Repolarization

Hikaru TANAKA,*[,a] Iyuki NAMEKATA,[a] Shogo HAMAGUCHI,[a] Taro KAWAMURA,[a] Hiroyuki MASUDA,[a] Yoshio TANAKA,[a,b] Naoko IIDA-TANAKA,[a,c] and Akira TAKAHARA[a]

[a] *Department of Pharmacology, Toho University Faculty of Pharmaceutical Sciences:* [b] *Department of Chemical Pharmacology, Toho University Faculty of Pharmaceutical Sciences: Funabashi, Chiba 274–8510, Japan: and* [c] *Department of Food Science, Otsuma Woman's University: Chiyoda-ku, Tokyo 102–8357, Japan.*
Received July 25, 2009; accepted October 21, 2009; published online October 22, 2009

Effects of NIP-142, a benzopyran compound which terminates experimental atrial arrhythmia, on potassium channel α-subunits and mouse atrial repolarization were examined. NIP-142 concentration-dependently blocked the outward current through potassium channel α subunits Kv1.5, Kv4.2 and Kv4.3 expressed in *Xenopus* oocytes. In isolated mouse atrial myocardia, NIP-142 prolonged the action potential duration and effective refractory period, and increased the contractile force. These results suggest that NIP-142 blocks the potassium channels underlying the transient and sustained outward currents, which may contribute to its antiarrhythmic activity.

Key words NIP-142; Kv1.5; Kv4.2; Kv4.3; atrial fibrillation

Atrial fibrillation is one of the most frequent types of arrhythmia and is reported to double the risk of deaths due to cardiovascular diseases. It is also the major risk factor for thromboembolism, especially cerebral embolism.[1] At present, atrial fibrillation is mainly treated with class I antiarrhythmic agents such as pilsicainide and flecainide, or class III antiarrhythmic agents such as dofetilide and amiodarone.[2–4] However, the major problem with these agents is that they also affect ventricular excitation and repolarization. Thus, drugs with atrial selectivity are desired for the treatment of atrial fibrillation.

NIP-142, (3*R**,4*S**)-4-cyclopropylamino-3,4-dihydro-2,2-dimethyl-6-(4-methoxyphenylacethylamino)-7-nitro-2*H*-1-benzopyran-3-ol, is a benzopyran derivative with terminating effects on canine vagal stimulation-induced atrial fibrillation model and on canine Y-shaped incision-induced atrial flutter model.[5] These effects have been attributed to prolongation of atrial refractory period. The prolongation of the refractory period and action potential duration (APD) by NIP-142 was observed in the atrium,[5,6] but not in the ventricle.[6] This may indicate that NIP-142 is less likely to disturb ventricular repolarization when applied for the treatment of atrial arrhythmia. In isolated human atrial cardiomyocytes, NIP-141, the hydrochloride salt of NIP-142, concentration-dependently inhibited the transient and sustained components of the outward current.[7] However, the molecular identity of the ion channels subject to inhibition has not yet been clarified. In the present study, we examined the effect of NIP-142 on expressed potassium channel α subunits Kv1.5, Kv4.2 and Kv4.3, which underlie the transient and sustained outward currents. As inhibitory effects were observed on these currents, we also examined the effect of NIP-142 on action potential duration, effective refractory period and contractile force in isolated mouse atrial myocardium. The effects of NIP-142 were compared with those of 4-aminopyridine to obtain information on the mechanism of action of NIP-142.

MATERIALS AND METHODS

Cloning of Mouse Kv1.5, Kv4.2 and Kv4.3 cDNA and Preparation of Specific cRNAs cDNA fragments for Kv1.5, Kv4.2 and Kv4.3 were amplified by polymerase chain reaction from a mouse heart cDNA library (Takara Shuzo Co., Ltd., Kyoto, Japan) with oligonucleotide primers designed based on the published mouse cDNA sequence of Kv1.5 (GenBank accession number AF108659), Kv4.2 (AF107780) and Kv4.3L (AF107781). The nucleotide sequence of the primers used for Kv1.5 were 5′-ATGCCCCTTGCCCCCGGGCCATGG-3′, 5′-GCTCTGCCAGCTCGGTGCCCAGGG-3′, 5′-TTTCTTTGCTTGCCCCAGCAAGGC-3′ and 5′-CAAGTCTGCCTCGATCTCTCTTTAC-3′, those for Kv4.2 were 5′-CAGACAACATGGCAGCCGGTGTTG-3′, 5′-AAGACTCCGCTCAGTGAGCAGATG-3′, 5′-AGCAAGCAAGTTCACCAGCATCCC-3′ and 5′-GCTCTCAGACCTGTGCCAATTGTC-3′, and those for Kv4.3 were 5′-CTGGAGTCACCATGGCGGCAGGAGTTG-3′, 5′-GGATGCTTGTGAACTTGCTGGCAG-3′, 5′-TGACCAACAATGAGGACGTGTCTG-3′ and 5′-CCCCCTCAGGCCCTCTGTCCAGTG-3′. These cDNA fragments were assembled with standard ligation techniques, and the full length cDNAs were separately inserted into the pGEM11Zf vector (Promega, Madison, WI, U.S.A.). The cRNAs for Kv1.5, Kv4.2 and Kv4.3 were obtained by *in vitro* transcription from linearized plasmid templates with mMESSAGE mMACHINE *in vitro* Transcription T7 kit (Ambion, Inc., Austin, TX, U.S.A.).

Oocyte Culture and Electrophysiological Assay *Xenopus laevis* oocytes were isolated from ovary lobes by collagenase treatment as described.[8] Then the oocytes were injected with cRNAs for Kv1.5, Kv4.2 or Kv4.3 (10 ng of each cRNA per oocyte) and were further incubated for 2—4 d until the electrophysiological assay. Two-electrode voltage clamp was performed as described[8] with OC-725 amplifier (Warner Instruments, Inc., Hamden, CT, U.S.A.) and glass microelectrodes filled with 3M KCl (0.5 to 2.0 MW). Oocytes were placed in a recording chamber perfused with ND96 solution

* To whom correspondence should be addressed. e-mail: htanaka@phar.toho-u.ac.jp

supplemented with $CaCl_2$ (composition in mM: NaCl 96, KCl 2, $MgCl_2$ 1, $CaCl_2$ 1.8, *N*-(2-hydroxyethyl)piperazine-*N'*-2-ethanesulfonic acid (HEPES) 5, pH 7.5). All experiments were performed at room temperature. Data acquisition and analysis were performed with pClamp software (Axon Institute).

Experiments with Isolated Mouse Atria All experiments with the mouse were approved by the Ethics Committee of Toho University, and were performed in accordance with the "Guiding Principles for the Care and Use of Laboratory Animals" approved by the Japanese Pharmacological Society. The left atria were isolated from ddy mice and measurement of the action potential with standard glass microelectrode techniques and measurement of contractile force were performed as described.[9] Measurement of the effective refractory period was performed by extracellular recording as previously described.[6]

Drugs and Chemicals NIP-142 was synthesized by Nissan Chemical Industries (Tokyo, Japan). NIP-142 was added to the bath solution from a stock solution (100 mM) in 0.1 M HCl. The final concentration of HCl in the measuring bath (<0.1 mM) did not affect any of the experimental parameters measured. All other chemicals were commercial products of the highest available grade of quality.

Statistical Analysis All experimental data are expressed as mean±standard errors of the mean (S.E.M.). The statistical significance of differences between means was evaluated by the paired *t*-test or the Dunnet's test for multiple comparisons as appropriate. A value of $p<0.05$ was considered statistically significant.

RESULTS

In *Xenopus* oocytes injected with the cRNAs for Kv1.5, Kv4.2 and Kv4.3, depolarization to membrane potentials more positive than −30 mV from a holding potential of −80 mV evoked outward currents. The Kv1.5 current showed rapid activation and very slow inactivation (Fig. 1A). The Kv4.2 and Kv4.3 currents showed rapid activation and inactivation (Figs. 1B, C). NIP-142, 10 μM and 100 μM, inhibited these outward currents both at the outward current peak and at the end of the 200 ms depolarizing pulse. The inhibition was concentration-dependent and statistically significant (Fig. 1D). The inhibition by 100 μM was larger with the Kv1.5 current. 4-Aminopyridine also inhibited these currents. At 100 μM, inhibition was observed only for the Kv1.5 channel current; the early phase outward current at 30 ms depolarization was reduced to 65.0±1.5% ($n=5$). At 1 mM, the Kv1.5, Kv4.2 and Kv4.3 channel currents (early phase or peak outward) were reduced to 12.4±3.2%, 85.0±3.1% and 92.8±2.7%, respectively ($n=5$). At 10 mM, all of these currents were completely inhibited.

The isolated mouse left atria had an action potential with short duration. 4-Aminopyridine induced a prolongation of the early phase repolarization (Fig. 2A) while tertiapin induced prolongation of the late phase (Fig. 2B). NIP-142 prolonged both the early and late phases of repolarization (Fig. 2C); the effect was concentration-dependent (Table 1). NIP-

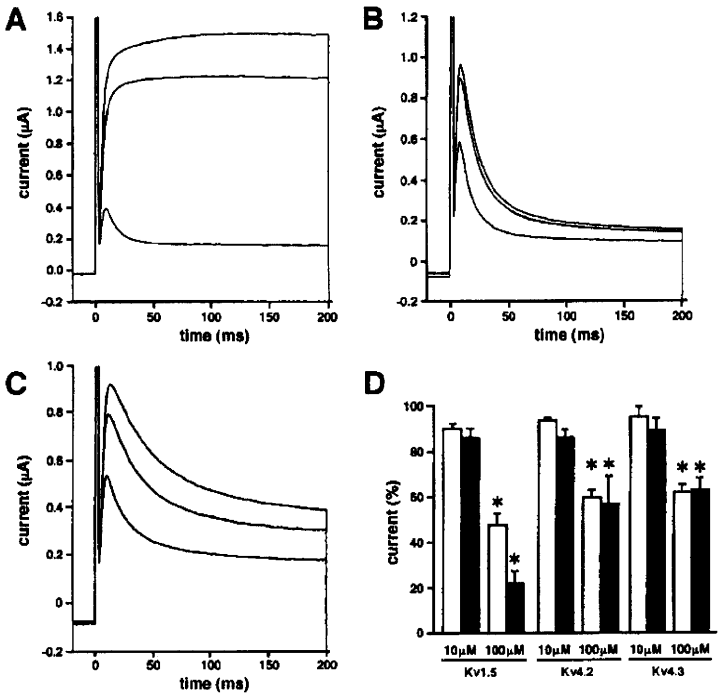

Fig. 1. Effect of NIP-142 on Potassium Channel Currents Expressed in *Xenopus* Oocytes

Typical current recordings for Kv1.5 (A), Kv4.2 (B), Kv4.3 (C) during 200 ms depolarizing voltage clamp pulses from −80 to +40 mV in the absence and presence of 10 μM and 100 μM NIP-142. Summarized results are shown in D. Columns and vertical bars indicate the mean±S.E.M. from 3 experiments. Open columns indicate the effects on the early phase (30 ms after depolarization for Kv1.5 and at the outward current peak for Kv4.2 and 4.3) and closed columns indicate those on the sustained current at the end of the depolarizing pulse. Asterisks indicate significant difference ($p<0.05$) from corresponding values before the application of NIP-142 as determined by the Dunnet's test for multiple comparisons.